Research Article

R. Saravanan, T. Sathish, V. Vijayan, S. Rajkumar, Shubham Sharma*, Changhe Li, Yanbin Zhang, Kamal Sharma, and Sayed M. Eldin*

Eco-friendly MoS_2/waste coconut oil nanofluid for machining of magnesium implants

https://doi.org/10.1515/rams-2022-0296
received September 25, 2022; accepted December 16, 2022

Abstract: The cost of the coolant and its disposal cost are significant issues in metal machining processes. In biocompatible magnesium alloy-based medical implants and instrument manufacturing, the cost hikes are owing to the use of unconventional machining processes and computerised numerical control machines. This research aims to improve machinability performance and optimize process parameters for biocompatible magnesium implant manufacturing for biomedical applications using eco-friendly nanofluid of MoS_2 nanoparticles suspended in waste coconut oil. The nanofluid was prepared from the multiple times used waste coconut oil (waste) and was mixed with MoS_2 nanoparticles. The orthogonal array L16, Taguchi analysis, and analysis of variance were employed in experimental design and statistical optimization. The machinability performance was determined by measuring and comparing the responses like cutting force, feed force, surface roughness, cutting zone temperature, and tool wear. They were compared with machining using a nanofluid and conventional commercial coolant. The results reveal that the proposed method of machining improved machinability performance appreciably; therefore, the observations of the proposed method were used and the process parameters were optimized. Mathematical models were developed for the prediction of process parameters. The proposed method exhibited the average reduction of the cutting force by 68.23167 N, feed force requirements by 34.180 N, the cutting zone temperature by 60.435°C, the surface roughness by 0.118908 μm, and the tool wear by 039938 $mg \cdot h^{-1}$.

Keywords: nanofluid, flood cooling, Taguchi, waste coconut oil, biomedical, magnesium implants

*** Corresponding author: Shubham Sharma,** Mechanical Engineering Department, University Center for Research & Development, Chandigarh University, Mohali, Punjab, 140413, India; School of Mechanical and Automotive Engineering, Qingdao University of Technology, 266520, Qingdao, China, e-mail: shubhamsharmacsirclri@gmail.com, shubham543sharma@gmail.com
*** Corresponding author: Sayed M. Eldin,** Center of Research, Faculty of Engineering, Future University in Egypt, New Cairo, 11835, Egypt, e-mail: elsayed.tageldin@fue.edu.eg
R. Saravanan: Department of Mechanical Engineering, Saveetha School of Engineering, S.I.M.A.T.S., Chennai 602 105, Tamil Nadu, India, e-mail: dr.sarravanan@gmail.com
T. Sathish: Department of Mechanical Engineering, Saveetha School of Engineering, S.I.M.A.T.S., Chennai 602 105, Tamil Nadu, India, e-mail: sathish.sailer@gmail.com
V. Vijayan: Department of Mechanical Engineering, K. Ramakrishnan College of Technology, Samayapuram, Trichy 621 112, Tamil Nadu, India, e-mail: vijayan.me@gmail.com
S. Rajkumar: Department of Mechanical Engineering, Faculty of Manufacturing, Institute of Technology, Hawassa University, Awasa, Ethiopia, e-mail: ccetraj@gmail.com
Changhe Li: School of Mechanical and Automotive Engineering, Qingdao University of Technology, 266520, Qingdao, China, e-mail: sy_lichanghe@163.com
Yanbin Zhang: School of Mechanical and Automotive Engineering, Qingdao University of Technology, 266520, Qingdao, China, e-mail: zhangyanbin1_QDLG@163.com
Kamal Sharma: Institute of Engineering and Technology, GLA University, Mathura (U.P.), 281406, India, e-mail: kamal.sharma@gla.ac.in

1 Introduction

Recently, alloys have been employed in manufacturing medical implants, particularly orthopaedic implants. In orthopaedic implants, biodegradable magnesium alloys are widely and usually preferred over stainless steel, titanium alloys, and cobalt-based alloys for avoiding undesirable outcomes like metal ion release and stress shielding as well as reducing the cost and weight [1]. For critical bone fracture, permanent alloy implants are needed and usually titanium alloys and steels are preferred, though they are expensive and heavy [2,3]. As Mg alloy is the lightest metal (1.738 $g \cdot cm^{-3}$ density [4]) and compatible with the structural application for bones (as critical bone density is in the range of 1.75–2.10 1.738 $g \cdot cm^{-3}$ [1]), in last decade the research on Mg alloys augmented 491% [5]. Pure Mg is less corrosive (407 $mm \cdot year^{-1}$) than its alloy form [6]. The Mg alloy with aluminium and zinc-reinforced composite was synthesized and tested for

biocompatibility and was found to be biocompatible [7]. Mg alloys are highly biodegradable and release hydrogen at approximately 0.01 $mL \cdot cm^{-2} \cdot day^{-1}$ [8,9]. In orthopaedic applications, usually, Mg is alloyed with Mn, Zn, Al, and Ca for use as biomaterials in place of pure Mg [10,11]. Young's modulus is one of the most important properties, which is merely considered for the selection of alternate for bone. The Young's modulus of human bone varies from 3 to 20 GPa and those of cobalt and chromium alloys were around 230 GPa, for titanium it ranged from 110 to 117 GPa, and for stainless steel, it ranged from 190 to 205 GPa; however, for Mg, it was 41–45 GPa, very close to the bone requirement [12,13]. Mg alloys are biocompatible, attractive, biodegradable, and possess appreciable mechanical properties [14–16]. They are light weight, less stress shielding, and their Young's modulus values are close to that of the bone. Moreover, Mg alloys have low corrosion resistance and hydrogen is released at the time of degradation [17]. The material design requirements differ from permanent metal implants [18]. The scientific aspects are biosafety (alloying agents like aluminium are avoided as they are toxic in the final form) and biocompatibility. The mechanical properties like tensile strength greater than 200 GPa, elongation limit of up to 10%, wear rate of less than 05 mm per year in human biofluid at body temperature, and also its biodegradation should be controlled; life time requirements are minimum 90 days and double of it as maximum [19]. The samples of circular cross-sectional implants are shown in Figure 1.

As with the selection of procurement source for procuring medically pure Mg, the selection of the manufacturing process is also essential. The selection includes machining accuracy, low cost of machining, harmless processing materials/chemicals used, and do not damage the implants thermally and chemically, and a search for mass production possibilities [19–26]. This research addresses the machining issue of circular-shaped implant manufacturing for meeting the above requirements.

The scientific evidence supports are presented in Table 1. The machinability could be improved by improving the tool hardness either by using coated tool [27,28] or by changing a much harder tool for machining. Alternatively, it can be done by reducing the tool wear. The tool wear could be reduced by supplying coolant and lubrication appropriately at the cutting zone. Coolant cost is one of the considerable costs in manufacturing. The literature suggested eco-friendly flood cooling [29], ultrasonically atomized cutting fluid [30], minimum quantity lubrication (MQL) [31,32], nanoparticles mixed flood cooling [33], hybrid nanoparticles mixed flood cooling, nanoparticles mixed MQL [34–39], hybrid nanoparticle mixed MQL [33,40–42], cryogenic cooling [43–45], and cryogenic/lubrication hybrid cooling [46].

The research gap can be stated as follows: all proposed methods in the above-discussed literature would lead to additional machining costs. The MQL is costlier than flood cooling and cannot be reused. The addition of nanoparticles in the MQL mode leads to the additional cost of the coolant. Nanoparticles may mix in the environmental air after drying the coolant if not cleaned properly.

Hence, this investigation was innovatively approached to develop a cheap and effective coolant from the waste resource. A reusable nanofluid developed from the waste coconut oil was assorted with MoS_2 nanoparticles to improve the machined surface quality, and reduce the tool wear, the cutting force, the feed force, and the cutting zone temperature. As this coolant contains edible oil, it is biodegradable and utilizes waste disposal. The performance of the proposed nanofluid is compared with the conventional coolant and it is found to be costlier. The commercial coolant was mixed with water. This coolant is 100% water-free and utilizes the used-edible oil of coconut oil (waste) for a valuable machining process.

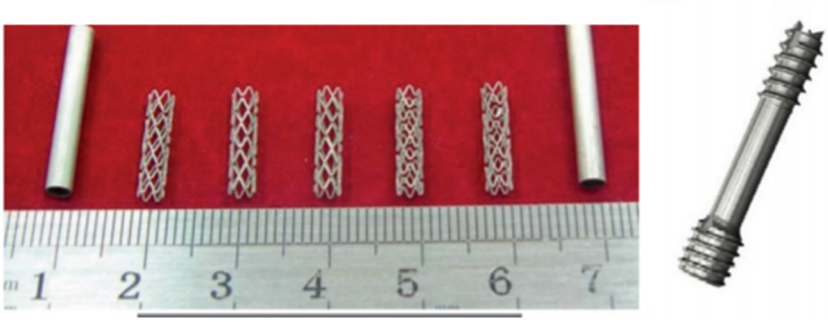

Figure 1: Samples of the circular implants.

Table 1: Some related observations from the existing literature

Problem	Intervention	Comparison	Outcome(s)	Ref.
Poor machinability of super duplex stainless steel	MQL for machining	Dry machining and flood, cooling	Low-stress corrosion cracking resistance	[31]
Poor machinability in C NC turning of AISI H13 tool steel	TiN-coated tool	Uncoated carbide tool for life tool wear	Less tool wear compared to the conventional uncoated carbide tool	[27]
Poor machinability of C NC turning of EN31 alloy steel	TiN-coated tool	Uncoated H SS tool	Higher chip thickness	[28]
Tool wear in machining titanium alloy Ti–6Al–4V	MQL for machining	Dry and flood coolant	The edge chipping and adhesion of chips to the cutting tools were reduced	[32]
Improper cooling at the cutting zone while machining alloys	Nano-additives: MQL for machining	Compared with MQL	Nano-additive-MQL system was found to be sustainable machining	[47]
To optimize the use of coolants instead of conventional flood cooling	MQL is composed of biodegradable oil with various nanoparticles for machining	Compared with dry and MQL	Achieved better surface finish, low power consumption, and fewer tool wear	[48]
To achieve environmentally sustainable manufacturing in pressure vessel carbon steel (SA516) using coated carbide inserts	MQL for machining	Compared with traditional flood coolant	Surface roughness and tool wear reduced significantly	[49]
Drilling on titanium	Cryogenic cooling conditions	Compared with traditional flood coolant	Drill maximum temperature reduced by 33–50%	[43]
Progressive tool wear while machining titanium alloy Ti6Al4V due to built-up edges, diffusion wear, and cutting forces	Cryogenic cutting with liquid nitrogen	Compared with conventional dry cutting and flood cutting	Eliminated the issues of BUE formation, diffusion wear, and cutting force fluctuation, especially under aggressive cutting conditions than flood cooling	[44]
Poor machinability for Ti–6Al–4V thin-wall components	Cryogenic MQL	MQL	Highly improved machinability, superior lubrication, and high cooling function	[45]
To develop sustainable and optimized machining of Ni-based industrial alloy	Adequate cooling/lubrication	Flood, MQL, and cryogenic	Improved surface quality and support for sustainable means of production	[46]
Machining of Hastelloy C-276	MQL for machining	Compared with conventional dry cutting and flood cutting	Cooling environment influencing cutting zone temperature, surface finish, and material removal rate	[50]
Oil mist generation and endanger the health of workers	Flood cooling	Oil mist mass concentrations in MQL	8.33–305.88 $mg{\cdot}m^{-3}$ in MQL, whereas 0.2–22.42 $mg{\cdot}m^{-3}$ in flood cooling	[29]
Poor surface quality in machining Hastelloy C-276	Ultrasonically atomized cutting fluid	Compared with conventional dry cutting and flood cutting	Surface quality improved by 20% than dry machining (17.4%)	[30]
Poor surface finish in grinding of 100Cr6-steel	SiO_2 nanofluids in MQL for machining	MQL	The surface finish improved significantly	[34]
Application of nanofluids for machining	Graphene oxide and paraffin- and soybean-based mixed with MoS_2 nanoparticles and hybrid nanofluids, namely alumina-multiwalled carbon nanotubes and alumina-graphene in the MQL form	MQL machining	Imparting superior lubrication and cooling effects under MQL machining	[51]
AA 2024 T3 Al alloy	Mineral oil-based MoS_2 nanofluid MQL	Dry cutting, base fluid MQL		[35]

(*Continued*)

Table 1: *Continued*

Problem	Intervention	Comparison	Outcome(s)	Ref.
			Built-up layer and built-up edge formation significantly reduced	
Poor surface integrity in internal-cooling-type grinding	MWCNTs and MoS_2/water-based coolant in flood cooling	Compared with conventional flood cutting	Considerably fewer burrs and furrows, temperature reduced by 3.61% and surface roughness reduced by 2.39%	[33]
MQL-milling of Inconel X-750 superalloy	Boron nitride/graphite nanoparticle-based nanofluid in MQL	Boron nitride/MoS_2 nanoparticle-based nanofluid graphite/MoS_2 nanoparticle-based nanofluid in MQL	Tool life improved by 36.17% compared with other combinations	[40]
Review on nanoparticles in coolant for machining processes	Hybrid nanoparticles	Mono nanoparticles	Nanoparticle concentration in the range of 0.25–0.5% (low and economical concentrations) is the most repetitive for optimal cases in most of the machining processes. Hybrid nanofluids show more positive effects compared with conventional nanofluids and base fluids. Cutting zone temperature, cutting force, tool wear, and surface roughness experience 10–40% and in some cases 50–70% positive change after applying nanoparticles in turning processes. Milling process and SiO_2, MoS_2, and graphene nanoparticles are reported as the most applied and effective ones	[41]
Tribological issues while turning AISI 420 hardened steel with cermet tools	Al_2O_3 and MoS_2	Conventional fluid (base fluid)	Significant synergistic effect	[42]
High surface roughness and tool wear in CNC. turning of 617 alloys by AlTiN PVD carbide cutting inserts	Al_2O_3 nanofluid in coconut oil under MQL condition	Optimization of cutting force, surface roughness, and tool wear	Surface quality improved and tool wear was reduced significantly	[52]

This research aims to develop a low-cost, high-performance nanofluid for machining biodegradable, biocompatible, and safe manufacturing of circular Mg implants with the use of eco-friendly nanofluid coolants. This research discusses improving the machinability performance and optimizing the process parameters for biocompatible magnesium implant manufacturing for biomedical applications with eco-friendly nanofluid of MoS_2 nanoparticles suspended in waste coconut oil. The machinability performances are observed under flood cooling conditions and compared with the conventional commercial coolant. Cutting fluid costs and the risk of disposing of them are major issues in flood cooling systems in metal machining processes. This investigation overcomes those issues by proposing to develop a coolant from the waste resource. Reusable nanofluid was developed from waste coconut oil and assorted with MoS_2 nanoparticles to improve the machined surface quality and reduce the tool wear, cutting force, feed force, and cutting zone temperature. As this coolant contains content edible oil, it is biodegradable. The performance of the proposed nanofluid is compared with conventional, costlier, and commercial coolant oil mixed with water. This coolant is 100% water-free and utilizes multiple times used edible coconut oil (waste) for a valuable machining process.

Hence, the novelty statement is to develop an effective nanofluid for flood cooling of machining Mg implants; it was prepared by mixing waste oil (used coconut oil) and MoS_2 nanoparticles at a low concentration, experimenting with a real-time application, statistically evaluating observations and comparing them with conventional coolant's performance, and then optimizing the process parameters for computerised numerical control (CNC) machining of Mg implants with the help of Taguchi analysis and analysis of variance (ANOVA). The research background, the literature review, the research gap, and the novelty of this

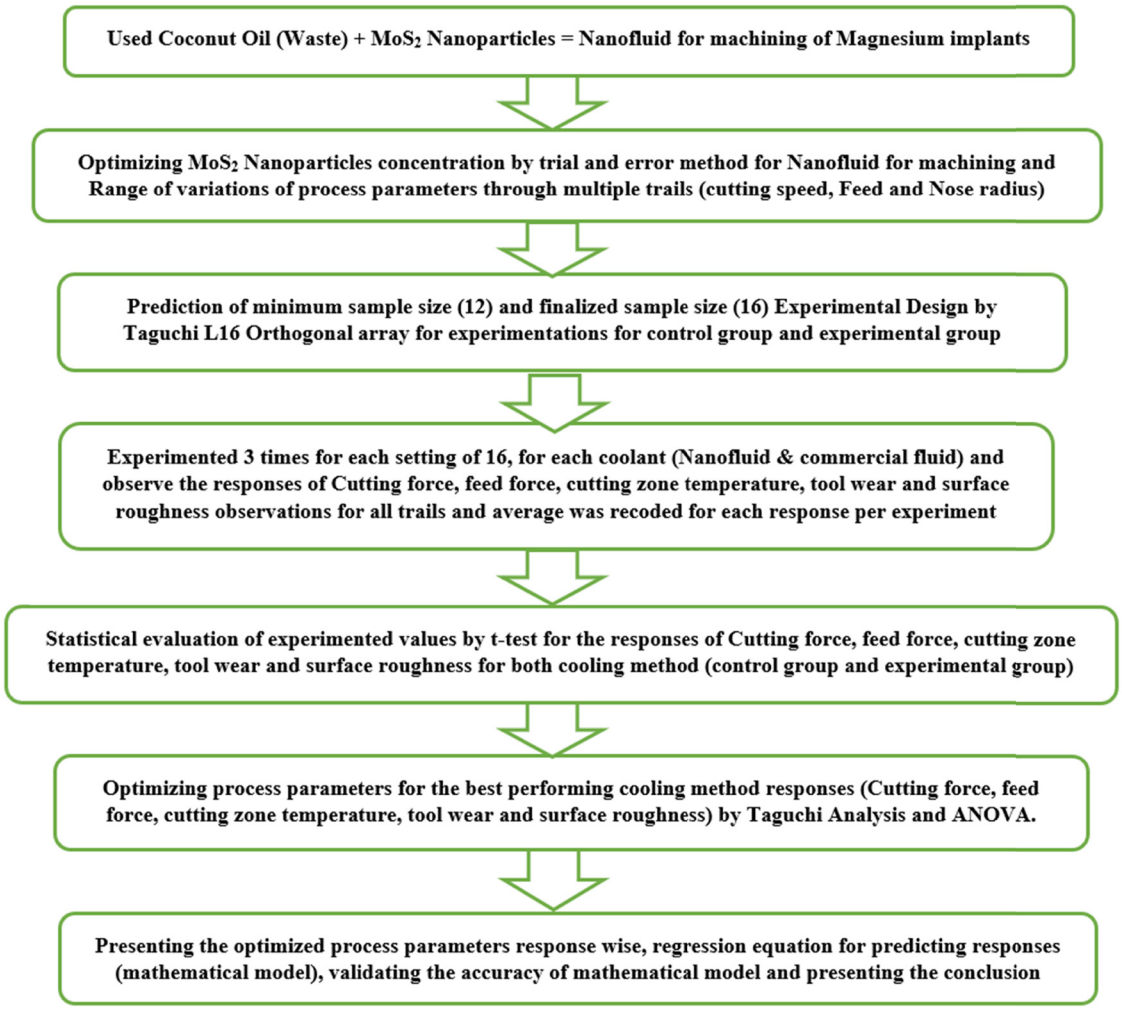

Figure 2: Research flow diagram.

investigation are presented in Section 1; the materials and research methods followed and observations are illustrated in Section 2. The results are analysed and optimized for minimizing cutting force, feed force, surface roughness, cutting zone temperature, and tool wear and explained in Section 4. The findings and conclusion are based on the results of the experimental observational analysis and are presented in Section 5.

2 Materials and methods

The flow of this investigation is presented in Figure 2. This investigation was carried out at the in-house research facility of high precision heavy duty (5HP) lathe (Figure 3).

The facility offers a high degree of accuracy in machining and can operate at eight different speeds in the range of 32–1,200 rpm and 18 variety automated feed (0.025–2.5 mm·rev^{-1}) conditions. Medically pure Mg rods were utilized as samples for testing the machinability. The round rods of the Mg workpiece material were purchased from Pujara High-Quality Steels Pvt. Ltd, Chennai. The mechanical properties of Mg implant materials, namely the density and elastic modulus of magnesium implants were 1.82 g·cm^{-3} and 43.5 GPa, respectively, and it is equivalent to the mechanical properties of bone [12,53,54]. The sample length of machining was 50 mm long. The conventional cutting fluid is Castrol make, Syntilo 9930 grade Downers Grove, Synthetic Coolant type IL mixed with 5% water. For preparing the nanofluid coolant, the MoS_2 nanoparticles were obtained from the chemical laboratory of Saveetha School of Engineering and reduced in particle size by grinding in a ball mill for 15 h. The waste coconut oil was obtained from Kerala Chips at Vadapalani, Chennai Branch, and filtered. The quantity of MoS_2 added was limited to the viscosity requirements of the coolant oil so that the pump power would not affect and the rated flow could be achieved. The waste coconut oil (used coconut oil) was filtered and then the impurities were removed. By the iterative test, the 30 g per 1,000 g of waste coconut oil ratio was finalized. The inclusion of MoS_2 not only improved the cooling and lubrication properties but also improved the fire point of the nanofluid. The nanofluid was prepared by mixing oil and nanoparticles of MoS_2 (<5 nm in size) in the ball mill for 12 h, which allows the nanoparticles to float on the mixed oil, which is a nanofluid. The coolant flow rate was set at 3.5 L·min^{-1} and it was ensured that no fumes were generated while cutting and the proposed oil is biodegradable. As no human sample is involved in this research, no ethical approval was required for this investigation. Hence, MoS_2 nanoparticles enriched with a waste coconut oil-based nanofluid in the flood-cooled machining process were verified and found to be very safe. The properties of the prepared nanofluid coolant were characterized and are furnished in Table 2. The mechanism behind the machining is cut by shearing and exposes the inner layer to the atmosphere at elevated temperatures [55,56]. If the water content coolant reacts with the surface, oxides may be produced and fumes generated. Hence, for this nanofluid, lubrication properties were considered to be a primary concern for the coolant (like coconut oil and MoS_2) preparation.

The heat was measured as the temperature at the cutting zone. The mercury pool thermocouple technique is employed for the temperature measurement; mercury was filled in the blue colour container (refer to Figure 3, left).

The force encountered while machining was measured with a lathe tool dynamo meter, which operates with 12 strain gauges. Each strain-gauge possesses 350 Ω resistance. The gauge factor is 2 ± 1. The set-up measures forces in three directions and converts them into net force acting on the tool as output.

The surface roughness was measured by using SURFTEST SJ-410. Figure 4 shows the surface roughness

Figure 3: Experimental set-up of HMT heavy-duty lathe with a tool dynamometer.

Table 2: Variable input parameters and their levels

Process variable	First level	Second level	Third level	Fourth level
Cutting velocity (m·min^{-1})	20	40	60	80
Tool feed (mm·rev^{-1})	0.025	0.050	0.075	0.100
Nose radius (mm)	0.30	0.60	0.90	1.20

Figure 4: SURFTEST SJ-410 surface roughness tester.

tester (Mitutoyo, Japan), which is a portable type surface roughness tester, employed to measure the surface roughness with a setting of 4 mm inspecting length, 0.5 mm·s^{-1} speed, 0.8 mm cut-off length, 2 mm nose radius, 600° angle of the tip, and 6 and 3.5 mm height and width of the stylus, respectively. The precision balance of LC 0.01 mg was utilized to measure the tool wear (in mg·h^{-1}) by dividing the machining time from the mass loss by the tool.

3 Experimentation

The limiting values of input variables are fixed with trails at various feeds, speeds, and depths of cut employed while finishing the shaft manufacturing in industries at Ambattur, Chennai. The variable input parameters are cutting velocity (in m·min^{-1}), nose radius (in mm), and feed rate (in mm·rev^{-1}). The range and levels of parameter variation are shown in Table 2 [57–61]. The carbide tip tool was employed in machining all samples in all kinds of cutting environments and the fresh tool was used in each experiment. The L16 type experimental design was used for the choice of the Taguchi experimental design for three factors at four levels. The experiments were conducted accordingly, and observations of the cutting force, feed force, surface roughness, cutting zone temperature, and tool wear were noted. All measurements were taken at five different locations/stages of processing of the workpiece after/during experiments, and the average was taken at each experiment [62,63]. The observations are consolidated for the control group in Table 3 and those for the intervention group in Table 4.

4 Results and discussions

The properties of the prepared nanofluid coolant were characterized and are given in Table 5. The machinability improvement was ensured by analysing the results with the help of independent sample tests and Taguchi and ANOVA procedures with the responses of cutting force, feed force, cutting zone temperature, surface roughness, and tool wear. The inputs are common except for the coolant of wet machining for the control group and intervention group.

4.1 *t*-Test

The machining performance was investigated for both machining methods by comparing the responses like cutting force, feed force, cutting zone temperature, surface roughness on machined surfaces, and wear of the tool. These results were statistically compared by performing one-way ANOVA, and a statistically significant difference

Table 3: Taguchi L16 experimental design type process inputs and experimental observations of the control group

Expt. no.	Cutting velocity ($m \cdot min^{-1}$)	Tool feed ($mm \cdot rev^{-1}$)	Nose radius (mm)	Cutting force (N)	Feed force (N)	Surface roughness (μm)	Cutting zone temperature (°C)	Tool wear ($mg \cdot h^{-1}$)
1	20	0.025	0.3	246.64	115.35	0.405	276.1	0.35
2	20	0.050	0.6	245.9	117.26	0.399	299.02	0.39
3	20	0.075	0.9	251.16	119.01	0.393	293.04	0.43
4	20	0.100	1.2	257.42	121.21	0.387	323.94	0.50
5	40	0.025	0.6	254.68	120.23	0.39	355.84	0.49
6	40	0.050	0.3	265.94	121.78	0.384	389.73	0.56
7	40	0.075	1.2	273.2	123.95	0.375	184.4	0.62
8	40	0.100	0.9	275.46	125.07	0.372	195.36	0.68
9	60	0.025	0.9	282.72	123.26	0.361	192.37	0.85
10	60	0.05	1.2	289.98	125.92	0.353	206.33	0.90
11	60	0.075	0.3	290.23	127.64	0.334	218.29	0.94
12	60	0.100	0.6	297.49	128.35	0.349	235.23	0.99
13	80	0.025	1.2	305.75	127.89	0.34	221.28	1.03
14	80	0.050	0.9	307.01	129.58	0.331	246.2	1.10
15	80	0.075	0.6	315.27	131.25	0.322	275.1	1.07
16	80	0.100	0.3	322.53	134.56	0.308	304.01	1.14

was observed for material removal rate ($p = 0.026$, $p < 0.05$). Table 4 shows group statistics that are the results of the *t*-test. From this table, it is clear that the average (mean) cutting force reduced from 280.0863 to 211.8546 N with the use of the proposed nanofluid in place of a conventional commercial coolant (Figure 5). Similarly, the mean feed force decreased from 124.5194 to 90.3394 N (Figure 6), the mean cutting zone temperature from 263.5150 to 203.0800°C (Figure 7), the mean surface roughness from 0.36278 to 0.24387 μm (Figure 8), and the mean tool wear from 0.7525 to 0.3531 $mg \cdot h^{-1}$ (Figure 9). The above-discussed values are their mean values; Table 6 shows the improvement in the machinability average by using a nanofluid-based coolant obtained from the machining practice than the dry machining practice.

Table 7 shows the results of the independent sample tests. It is evident from the table that the observations are significant, i.e. they did not violate statistical

Table 4: Taguchi L16 experimental design type process inputs and experimental observations of the intervention group

Expt. no.	Cutting velocity ($m \cdot min^{-1}$)	Tool feed ($mm \cdot rev^{-1}$)	Nose radius (mm)	Cutting force (N)	Feed force (N)	Surface roughness (μm)	Cutting zone temperature (°C)	Tool wear ($mg \cdot h^{-1}$)
1	20	0.025	0.3	132.98	85.03	0.272	175.04	0.06
2	20	0.05	0.6	142.1	86.98	0.268	180.76	0.08
3	20	0.075	0.9	148.42	87.73	0.263	185.46	0.13
4	20	0.100	1.2	157.54	88.33	0.256	189.14	0.18
5	40	0.025	0.6	170.42	87.55	0.263	182.18	0.21
6	40	0.05	0.3	179.3	88.94	0.257	190.76	0.24
7	40	0.075	1.2	189.61	89.35	0.252	197.13	0.29
8	40	0.100	0.9	215.61	90.11	0.248	202.32	0.33
9	60	0.025	0.9	216.87	90.98	0.249	199.34	0.34
10	60	0.050	1.2	229.79	91.16	0.24	205.25	0.39
11	60	0.075	0.3	246.38	92.72	0.231	213.32	0.44
12	60	0.100	0.6	258.33	93.55	0.233	221.26	0.50
13	80	0.025	1.2	266.16	91.97	0.227	210.78	0.53
14	80	0.050	0.9	274	92.34	0.221	221.26	0.58
15	80	0.075	0.6	276.22	93.81	0.215	231.42	0.64
16	80	0.100	0.3	285.94	94.88	0.207	243.86	0.71

Table 5: Thermophysical properties of waste coconut oil/MoS_2 nano-coolant

Description of properties	Value
Viscosity	368 cS at 21°C
pH	9.6
Thermal conductivity	1,356 $W{\cdot}m^{-1}{\cdot}K^{-1}$
Surface tension	68 $mN{\cdot}m^{-1}$
Wettability	Good
Density	1,087 $kg{\cdot}m^{-3}$
Flash point	>500°C

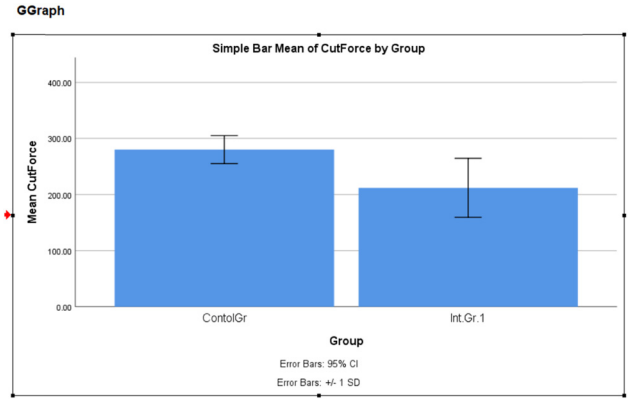

Figure 5: G-graph output comparing the mean values of the cutting force encountered at a 95% confidence level and error ±1% in the control group and the intervention group.

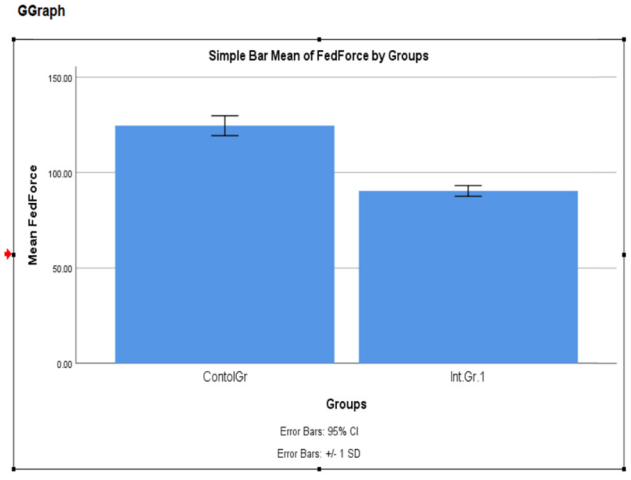

Figure 6: G-graph output comparing the mean values of the feed force encountered at a 95% confidence level and error ±1% in the control group and the intervention group.

assumptions. As the value of significance (p) is 0.001 and it is less than 0.05, for cutting force observations of both groups (control and intervention groups), it can be

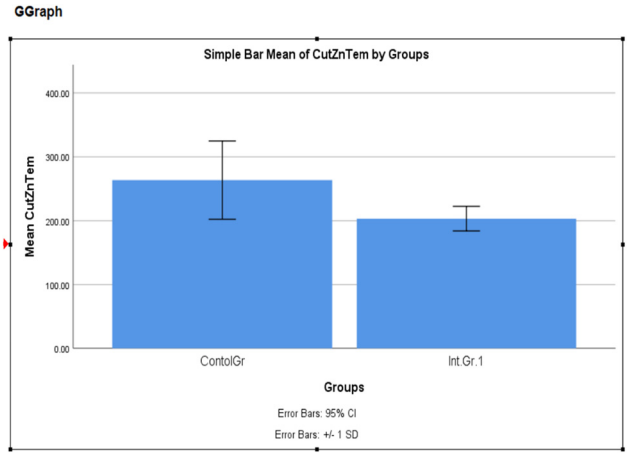

Figure 7: G-graph output comparing the mean values of the cutting zone temperature encountered at a 95% confidence level and error ±1% in the control group and the intervention group.

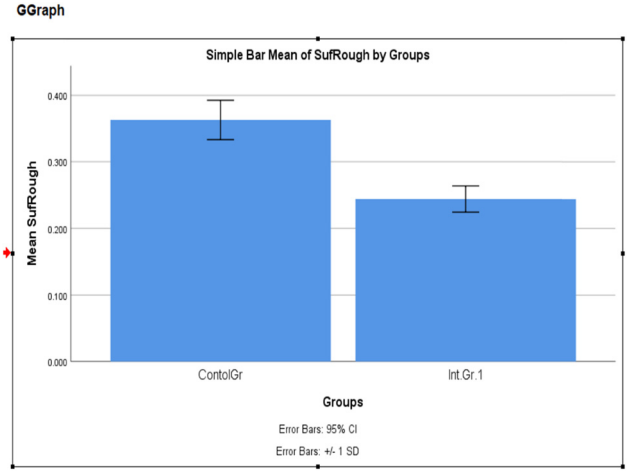

Figure 8: G-graph output comparing the mean values of the surface roughness encountered at a 95% confidence level and error ±1% in the control group and the intervention group.

confirmed that the observations obey statistical assumptions and are acceptable. Similarly, the significance value (p) is 0.023 ($p < 0.05$) for feed force observations.

It was observed that $p = 0.0001$ and $p < 0.05$ for the cutting zone temperature; $p = 0.045$ ($p < 0.05$) for surface roughness; and $p = 0.028$ ($p < 0.05$) for tool wear. Hence, observations were significant and acceptable as per the results of the independent sample tests.

As shown in Table 7, the positive mean values comparatively decrease the respective values than in the control group. It is understood that the cutting force at $t_{4.682} = 68.23167$ N, i.e. 68.23167 N cutting force, averagely reduced with the use of the proposed nanofluid in place of a conventional commercial coolant; similarly, the feed

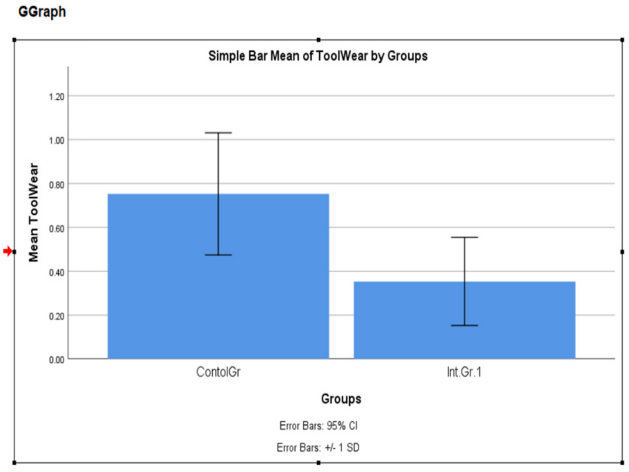

Figure 9: G-graph output comparing the mean values of tool wear encountered at a 95% confidence level and error ±1% in the control group and the intervention group.

force at $t_{22.933}$ = 34.18000 N, cutting zone temperature at $t_{3.758}$ = 60.43500°C, surface roughness at $t_{13.319}$ = 0.118908 µm, and tool wear $t_{4.660}$ = 0.39938 mg·h^{-1}. Hence, the proposed method of processing significantly improved machinability.

Figure 5 shows the G-graph output by comparing the mean values of the cutting force encountered at a 95% confidence level and error ±1% in the control group and the intervention group. Similarly, Figures 6–9 show the G-graph output by comparing the mean values of the feed force, cutting zone temperature, surface roughness, and tool wear.

The minimum value of the responses, such as responses of the cutting force, feed force, cutting zone temperature, tool wear, and surface roughness, are preferred in the machining metals in the CNC lathe; therefore, the minimum value is best for obtaining the high-quality product, safe and reliable performance for a long time too [64–66]. Here, the optimization is to minimize the responses of the cutting force, feed force, cutting zone temperature, tool wear, and surface roughness, and the above-said responses are considered. In this investigation, it was suggested to minimize the responses; Hussain [53] and Naqiuddin *et al.* [54] proposed using the following signal-to-noise (S/N) ratio equation, where smaller values are preferred:

$$\frac{S}{N_j} = -10\log \sum_{v=1}^{N_j} \frac{y_v^2}{N_j}, \tag{1}$$

where the number of trails is expressed as N_j, and the subscripts j and v denote the trail and test values.

4.2 Taguchi analysis of the cutting force

Taguchi analysis gives the degree of possibilities to achieve the objective function. Here, the objective is to minimize the cutting force (the smaller the better) [21–26,67–70]. For this statistical model, the intervention group observations of cutting forces on 16 different experiments were used to optimize the proposed method. Figure 10 shows the main effect plots for the signal-to-noise ratio for the response observations of the cutting force during experiments with the proposed nanofluid. The above mean line indicates large signals (possibilities towards the objective function of reducing the cutting force) and the left-most graph for the cutting velocity shows an increase of the cutting force with the increase of the cutting velocity; in other words, a decrease of possibilities (signals) in minimizing the cutting force [71–73]. The decision could be made based on the highest signal-to-noise ratio. Hence, the input setting of the cutting velocity of 20 m·min^{-1} (S/N = –43.23), the feed

Table 6: Group statistics results of *t*-tests

Group statistics					
	Groups	***N***	**Mean**	**Std. deviation**	**Std. error mean**
Cutting force	Control group	16	280.0863	25.14723	6.28681
	Intervention group 1	16	211.8546	52.59007	13.14752
Feed force	Control group	16	124.5194	5.264080	1.31602
	Intervention group 1	16	90.3394	2.798510	0.69963
Cutting zone temperature	Control group	16	263.5150	61.28352	15.32088
	Intervention group 1	16	203.0800	19.53427	4.88357
Surface roughness	Control group	16	0.36278	0.029805	0.007451
	Intervention group 1	16	0.24387	0.019671	0.004918
Tool wear	Control group	16	0.7525	0.278270	0.06957
	Intervention group 1	16	0.3531	0.200190	0.05005

Table 7: Results of independent sample tests

Independent sample tests										
		Levene's test for equality of variances		*t*-Test for equality of mean						
		F	Sig.	*t*	DF	Sig. (2-tailed)	Mean difference	Std. error difference	95% confidence interval of the difference	
									Lower	Upper
Cutting force	Equal variances assumed	12.780	0.001	4.682	30	0.000	68.23167	14.57330	38.46901	97.99432
	Equal variances not assumed			4.682	21.519	0.000	68.23167	14.57330	37.96925	98.49409
Feed force	Equal variances assumed	5.746	0.023	22.933	30	0.000	34.18000	1.49043	31.13613	37.22387
	Equal variances not assumed			22.933	22.852	0.000	34.18000	1.49043	31.09570	37.26430
Cutting zone temperature	Equal variances assumed	18.361	0.000	3.758	30	0.001	60.43500	16.08038	27.59448	93.27552
	Equal variances not assumed			3.758	18.017	0.001	60.43500	16.08038	26.65365	94.21635
Surface roughness	Equal variances assumed	4.372	0.045	13.319	30	0.000	0.118908	0.008928	0.100675	0.137141
	Equal variances not assumed			13.319	25.983	0.000	0.118908	0.008928	0.100556	0.137260
Tool wear	Equal variances assumed	5.311	0.028	4.660	30	0.000	0.39938	0.08570	0.22435	0.57440
	Equal variances not assumed			4.660	27.246	0.000	0.39938	0.08570	0.22361	0.57514

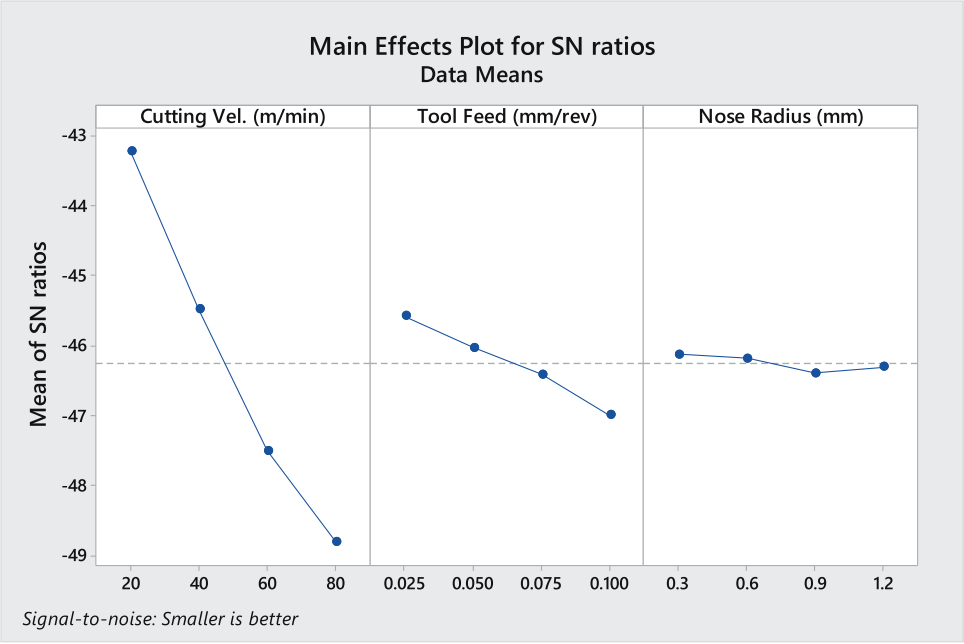

Figure 10: Main effect plots for the signal-to-noise ratio for the response observations of the cutting force during experiments with the proposed nanofluid.

rate of 0.025 mm·rev^{-1} (S/N = −45.58), and the nose radius tool of 0.3 mm (S/N = −46.13) gave a minimum cutting force (Figure 10). The variability is found to be higher in the cutting velocity input than in the tool feed and significantly less in the nose radius of the tool used [74–76]. Table 8 shows the results of the Taguchi analysis, which is the yield of S/N ratios.

Table 8 shows the classification of the process parameters based on their influence according to the delta value obtained in this statistical analysis. The higher delta value indicates a higher influence based on the delta value ranking of the process variable determined. As the delta value for the cutting velocity is 5.58 and greater than the data value of the tool feed and nose radius factors, the cutting velocity is the no. 1 factor (Rank 1) and influences the cutting force while machining. Accordingly, Rank 2 is for the tool feed (delta = 1.41) and Rank 3 is for the nose radius of the tool.

Table 8: Taguchi analysis results for the observation of the cutting force

Level of factors	Signal-to-noise ratio (the smaller the better)		
	Cutting velocity (m·min^{-1})	Tool feed (mm·rev^{-1})	Nose radius (mm)
1	−43.23	−45.58	−46.13
2	−45.48	−46.03	−46.19
3	−47.51	−47.00	−46.40
4	−48.80	−46.41	−46.31
Delta	5.58	1.41	0.27
Rank	1	2	3

4.3 ANOVA results on the response of the cutting force

The residual plots for cutting force observations are shown in Figure 11. The normal probability plot shows the quality of observations [77–82]. No observations deviate much from the mean line and residual error in these observations. Hence, it is concluded that the observations are not violating the statistical assumption and are ensured as valid.

Table 9 shows the results of the ANOVA on the response of the cutting force for the decision on the influence of factors. In this stage, one can decide the factor level based on the p-value. Here, a minimum p-value indicates more influence. The decision criteria are as follows: if $p < 0.05$, the factor is significantly influencing the measured response, and $p > 0.1$ indicates an insignificant factor [83–85]. From the Taguchi analysis, it was observed that the cutting force was of Rank 1 and the significant value was 0.001 (very low); similarly, $p = 0.004$ ($p < 0.05$) for the tool feed. But, in the case of the nose radius, $p = 0.940$ ($p > 0.1$), so it was found to be insignificant.

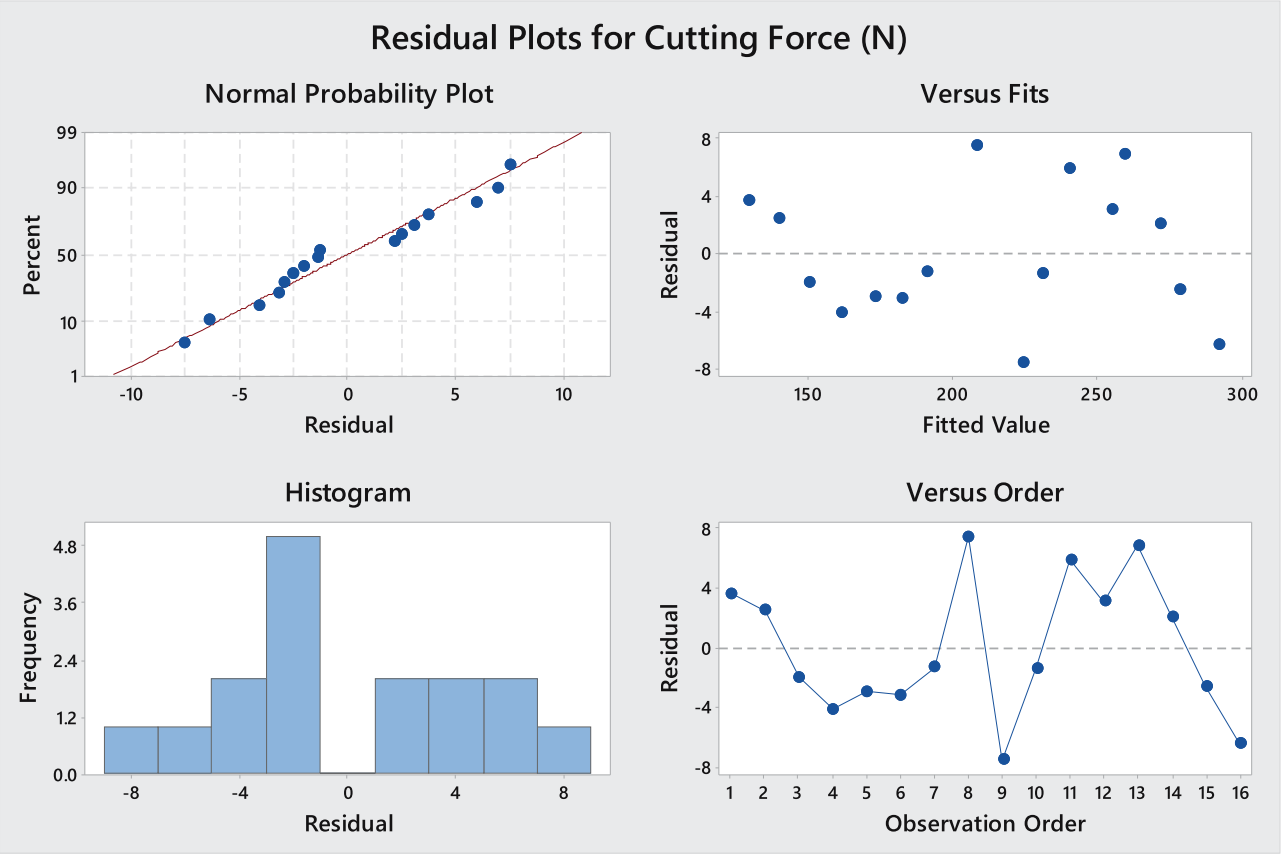

Figure 11: Residual plot for cutting force observations.

Table 9: Results of the ANOVA on the response of the cutting force for a decision on influencing factors

Source	DF	Adj SS	Adj MS	*F*-Value	*p*-Value
Cutting velocity (m·min^{-1})	3	38822.6	12940.9	240.72	0.000
Tool feed (mm·rev^{-1})	3	2322.1	774.0	14.40	0.004
Nose radius (mm)	3	20.7	6.9	0.13	0.940
Error	6	322.6	53.8		
Total	15	41488.0			

Table 9 shows the results of ANOVA at factor-level decision-making. This is a process that can be controlled for meeting the cutting force by altering the independent variables in which a highly sensitive independent variable has a low value of p; in other words, the independent variable which contributes more to alter the response of the cutting force has a higher F value [86–88]. Hence, the high contribution (F-240.72), a highly sensitive independent variable, is the cutting velocity (as $F = 240.72$ and $p = 0.001$ in Table 9). The next is the tool feed. But the nose radius is not significant as $p = 0.940 > 0.10$ [89–91], which means the change in the nose radius does not affect the cutting force considerably [92–94]. Hence, the contribution is very low ($F = 0.13$).

The table of coefficients is shown in Table 10, from which one can take a deep decision on the degree of influence of factor at its level of input. Similar to Table 9, here the p-value indicates the significance of the level of factors on the response. From this output, the influence factors can be observed. As $p > 0.1$, the tool feed of 0.050 mm·rev^{-1} ($p = 0.131$) and nose radii of 0.3 mm ($p = 0.832$), 0.6 mm ($p = 0.979$), and 0.9 mm ($p = 0.577$) are not significant, as the nose radius does not influence. The relation between the tool feed rate and cutting speed is depicted on the three-axis graphs surface plot in Figure 12. From this plot, the combined effects of both variables on the response of the cutting force at the cutting zone can be understood.

4.4 Regression equation

The regression equation was developed based on the coefficients obtained in the ANOVA, and the results are

Table 10: Results of ANOVA on the response of the cutting force for the decision on influence factors

Term	Coefficient	SE coefficient	*T*-value	*p*-Value	V IF
Constant	211.85	1.83	115.58	0.000	
Cutting velocity (m·min^{-1})					
20	−66.59	3.17	−20.98	0.000	1.50
40	−23.12	3.17	−7.28	0.000	1.50
60	25.99	3.17	8.19	0.000	1.50
Tool feed (mm·rev^{-1})					
0.010	17.50	3.17	5.51	0.001	1.50
0.025	−15.25	3.17	−4.80	0.003	1.50
0.050	−5.56	3.17	−1.75	0.131	1.50
Nose radius (mm)					
0.3	−0.70	3.17	−0.22	0.832	1.50
0.6	−0.09	3.17	−0.03	0.979	1.0
0.9	1.87	3.17	0.59	0.577	1.50

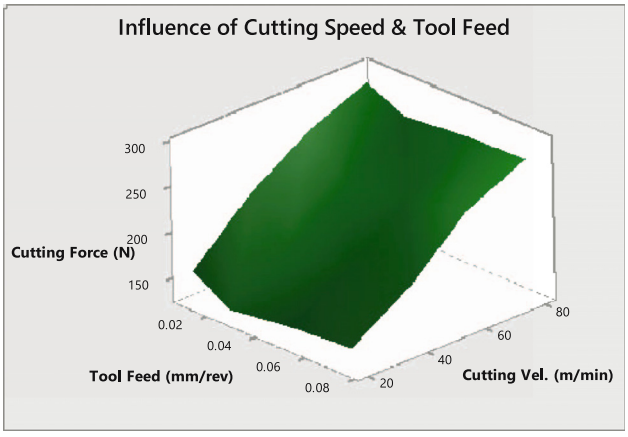

Figure 12: A 3D surface plot showing the relationship between the tool feed and cutting velocity in cutting force response.

shown in Table 11. The mathematical model is a mathematical equation from which anyone can interpret values of untested combinations or predict the process parameter levels for the desired response [95–97]. The developed regression model is given as follows:

Table 11: Model summary for the Taguchi analysis on the cutting force response

S	R^2	R^2 (adj)	R^2 (pred)
7.33211	99.22%	98.06%	94.47%

the cutting force. The factor cannot be taken into account here as it is insignificant for the cutting force.

ANOVA results for validation of a statistical model for the cutting force response can be noticed from the R^2 value from the model summary (Table 8). The condition is that the R^2 value must be greater than 95% for a good model; in this case, the value of R^2 is 99.22% and hence the model is acceptable. It also indicates that there is a good agreement between the predicted and experimented values.

4.5 Taguchi analysis of the feed force

As known, Taguchi analysis offers some degree of possibility to achieve the objective of the function. Here, the aim is to minimize the feed force (smaller the best). For this statistical model, the intervention group observations of cutting forces on 16 different experiments were used to optimize the process parameters.

Figure 13 shows the main effect plots for the signal-to-noise ratio for the response observations of the feed force during experiments with the proposed nanofluid. Figure 13 shows that a higher S/N ratio implies the best possibility for obtaining a low feed force at a cutting velocity of 20 m·min^{-1}, a feed rate of the tool of 0.025 mm·rev^{-1} , and a nose radius tool of 0.9 or 1.2 mm. The ambiguity of the nose radius tool selection is clarified in Table 12. Level 4 has the highest signal-to-noise ratio of −39.10 in comparison with both Levels 1 and 3, respectively.

$$\begin{aligned}\text{Cutting force(N)} = {} & 211.85 - 66.59*[\text{cutting vel.(m·min}^{-1}\text{)\_20}] - 23.12\,8[\text{cutting vel.(m·min}^{-1}\text{)\_40}] \\ & + 25.99*[\text{cutting vel.(m·min}^{-1}\text{)\_60}] + 63.73*[\text{cutting vel.(m·min}^{-1}\text{)\_80}] \\ & + 17.50*[\text{tool feed(mm·rev}^{-1}\text{)\_0.010}] - 15.25*[\text{tool feed(mm·rev}^{-1}\text{)\_0.025}] \\ & - 5.56*[\text{tool feed(mm·rev}^{-1}\text{)\_0.050}] + 3.30*[\text{tool feed(mm·rev}^{-1}\text{)\_0.075}] \\ & - 0.70*[\text{nose radius(mm)\_0.3}] - 0.09*[\text{nose radius(mm)\_0.6}] \\ & + 1.87*[\text{nose radius(mm)\_0.9}] - 1.08*[\text{nose radius(mm)\_1.2}].\end{aligned} \tag{2}$$

The 3D surface plot (Figure 11) exhibits the relationship between the cutting velocity and tool feed inputs on

So, a 1.2 mm radius offers a minimum feed force at the cutting zone.

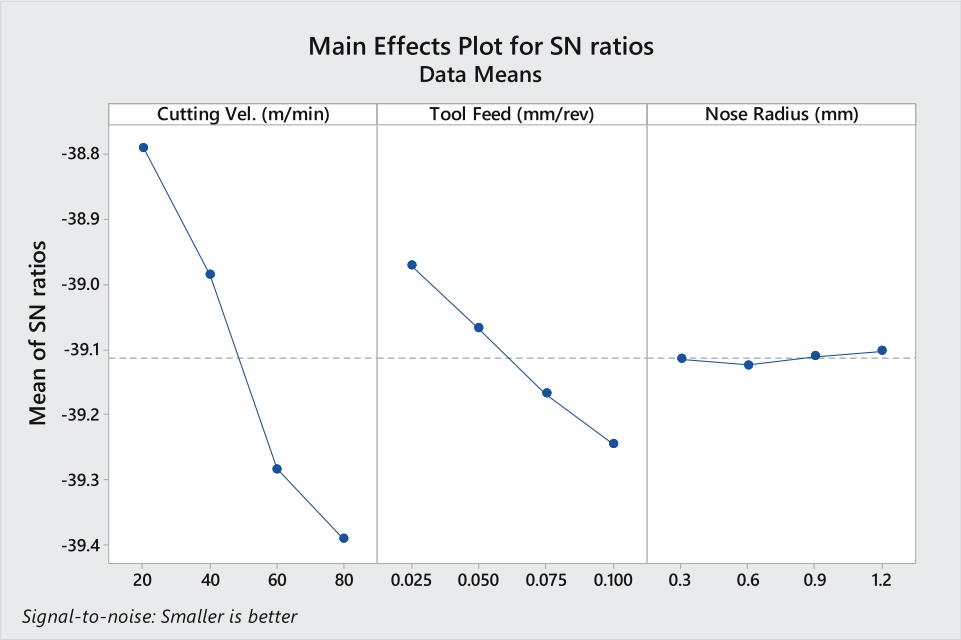

Figure 13: Main effect plots for the signal-to-noise ratio of feed force response observations during experiments with the proposed nanofluid.

The mean line in Figure 13 indicates large signals (possibilities towards the objective function of reducing the feed force); the left-most graph for the cutting velocity shows an increase of feed force with the increase of cutting velocity; in other words, a decrease of possibilities (signals) in minimizing the feed force [98–100]. Hence, the input setting of 20 $m \cdot min^{-1}$ cutting velocity, 0.025 $mm \cdot rev^{-1}$ feed rate, and 0.3 mm nose radius tool gave a minimum feed force. The variability is found to be high in the cutting velocity input than in the tool feed and very low in the nose radius of the tool used [101–103]. Table 12 shows the results of the Taguchi analysis, which is the yield of S/N ratios.

Table 12 describes the process parameters based on their influence according to the delta value obtained statistically. The higher delta value indicates a higher influence based on the delta value ranking of the process variable determined. As the delta value for the cutting velocity is 0.6, which is greater than the data values of tool feed and nose radius factors, the cutting velocity is the no. 1 factor (Rank 1) influencing the feed force while machining. Accordingly, Rank 2 is for the tool feed (delta = 0.27), and Rank 3 is for the nose radius of the tool (delta = 0.02).

Table 12: Taguchi analysis results for the observation of the feed force

Level	Cutting velocity ($m \cdot min^{-1}$)	Tool feed ($mm \cdot rev^{-1}$)	Nose radius (mm)
1	−38.79	−39.25	−39.12
2	−38.99	−38.97	−39.12
3	−39.28	−39.07	−39.11
4	−39.39	−39.17	−39.10
Delta	0.60	0.27	0.02
Rank	1	2	3

4.6 ANOVA results on the response of the feed force

The residual plots for feed force observations are shown in Figure 14. The normal probability plot shows the quality of observations. No observations deviate much from the mean line, and residual errors in these observations are in an acceptable range. But only one observation out of 16 was found to deviate (Table 13). Hence, observational accuracy was ensured from the statistical output of ANOVA, as shown in Figure 14.

The results of the ANOVA on the response of the feed force for a decision on the influence of factors are explained in Table 14. In this stage, one decides factor-level decisions based on the p-value. Here, a minimum p-value indicates more influence. The decision criteria are as follows: if $p < 0.05$, the factor is significantly influencing

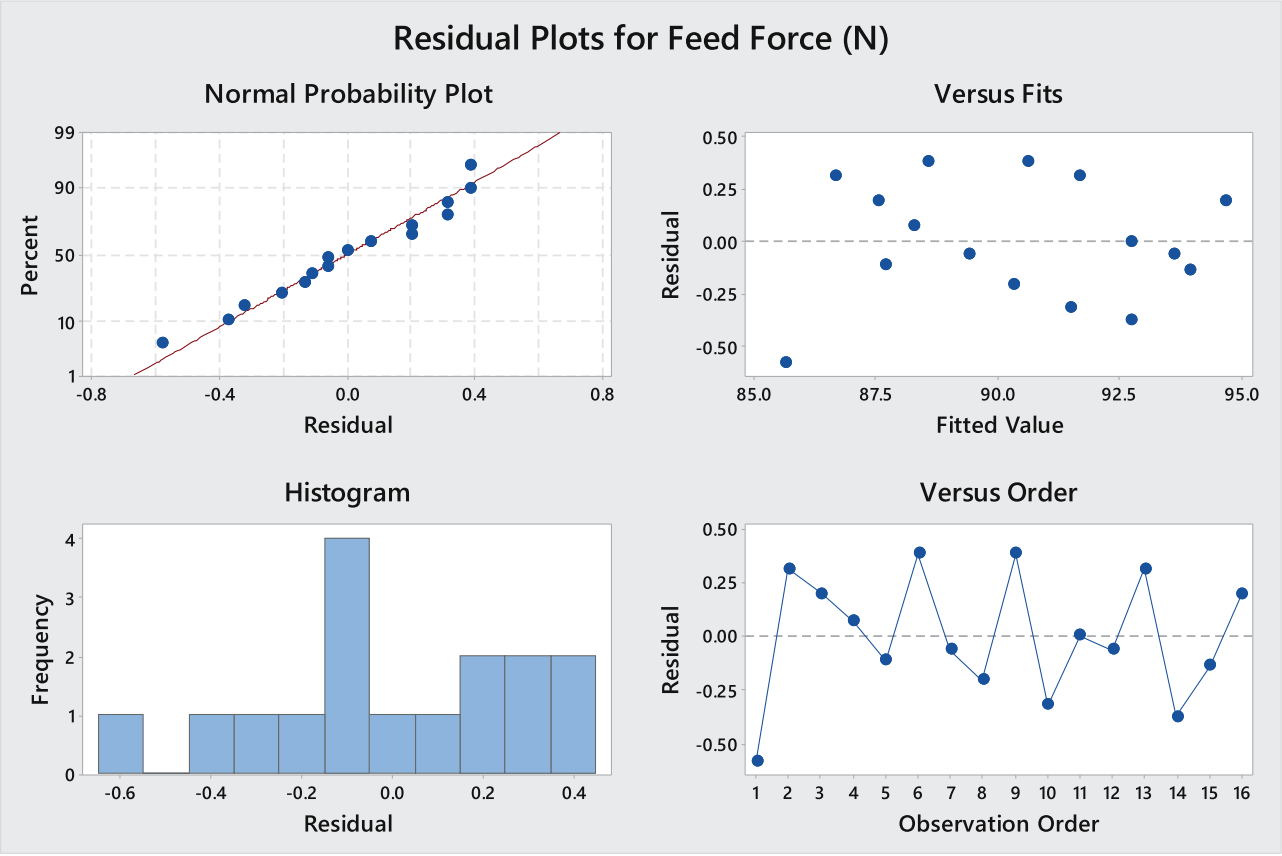

Figure 14: Residual plot for feed force observations.

Table 13: Fits and diagnostics for unusual observations of the feed force

Obs	Feed force (N)	Fit	Residual	Std residual	
1	85.030	85.614	−0.584	−2.09	*R* is a large residual

the measured response; $p > 0.1$ indicates an insignificant factor. From Taguchi analysis, it was observed that the feed force was of Rank 1 and the significant value was 0.001 (very low); similarly, $p = 0.001$ ($p < 0.05$) for the tool feed. But, in the case of nose radius, $p = 0.846$ ($p > 0.1$) so it was found to be insignificant. Table 14 shows the results of ANOVA at factor level decision making. It can be understood from Table 14 that for controlling the process for obtaining the desired response of feed force, alter the cutting velocity than the tool feed rate. There is no use in varying the tool inserts with different nose radii [104–106].

Table 14: Results of ANOVA for the analysis on the influence of factors

Source	DF	Adj SS	Adj MS	*F*-value	*p*-Value
Cutting velocity ($m \cdot min^{-1}$)	3	97.771	32.5904	157.29	0.000
Tool feed ($mm \cdot rev^{-1}$)	3	18.294	6.0979	29.43	0.001
Nose radius (mm)	3	0.167	0.0556	0.27	0.846
Error	6	1.243	0.2072		
Total	15	117.475			

The table of coefficients is shown in Table 15, from which one can take a deep decision on the degree of the influence of the factor at its level of input. Similar to Table 14, here, the *p*-value indicates the significance of the level of factors on the response. Table 15 gives much insight into the above decision that variation of tool feeds up to 0.025 is better than the range 0.025–0.050 for reduction of the feed force on the tool. Figure 15 shows the 3D surface plot of the relationship between the tool feed and cutting velocity in the feed force response.

Table 15: Results of ANOVA on the response of the cutting force for a decision on the influence at the level of factors

Term	Coefficient	SE coefficient	*T*-Value	*p*-Value	VIF
Constant	90.339	0.114	793.86	0.000	
Cutting velocity (m·min^{-1})					
20	−3.322	0.197	−16.85	0.000	1.50
40	−1.352	0.197	−6.86	0.000	1.50
60	1.763	0.197	8.95	0.000	1.50
Tool feed (mm·rev^{-1})					
0.010	1.378	0.197	6.99	0.000	1.50
0.025	−1.457	0.197	−7.39	0.000	1.50
0.050	−0.484	0.197	−2.46	0.049	1.50
Nose radius (mm)					
0.3	0.053	0.197	0.27	0.797	1.50
0.6	0.133	0.197	0.68	0.525	1.50
0.9	−0.049	0.197	−0.25	0.811	1.50

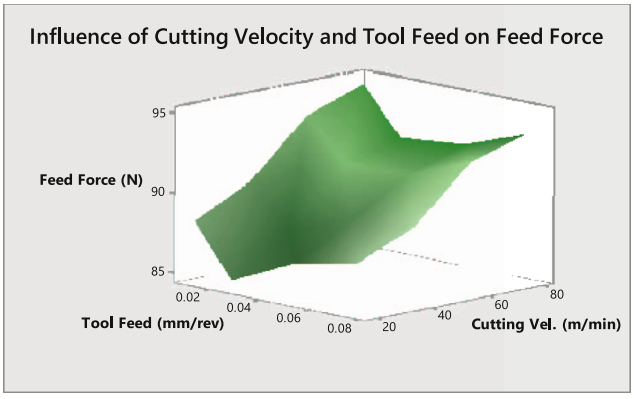

Figure 15: A 3D surface plot showing the relationship between the tool feed and cutting velocity in the feed force response.

4.7 Regression equation

Table 15 mainly helps to form the mathematical model by generating the regression equation. The mathematical model helps one to interpret values of untested combinations or predict the process parameter levels for the desired response. The regression model is given as follows:

summary (Table 16). The condition is that the R^2 value must be greater than 95% for a good model; in this case, the R^2 value is 98.94% and hence the model is acceptable. As $R^2 > 95\%$, the regression equation is reliable and its prediction accuracy is high.

4.8 Taguchi analysis on the surface roughness

Taguchi analysis gives the degree of possibilities to achieve the objective function. Here, the objective is to minimize the surface roughness (the smaller the better). For this statistical model, the intervention group observations of the surface roughness in 16 different experiments were used to optimize the proposed method. Figure 16 shows the main effect plots for the signal-to-noise ratio for the response observations of the surface roughness during experiments with the proposed nanofluid. The mean line indicates large signals (possibilities towards the objective function of reducing the surface roughness), and the right-most graph for the cutting velocity shows that with an increase of surface roughness,

$$\begin{aligned}\text{Feed force(N)} = {} & 90.339 - 3.322\,\text{cutting vel.(m·min}^{-1}\text{)\_20} - 1.352\,\text{cutting vel.(m·min}^{-1}\text{)\_40} \\ & + 1.763\,\text{cutting vel.(m·min}^{-1}\text{)\_60} + 2.911\,\text{cutting vel.(m·min}^{-1}\text{)\_80} \\ & + 1.378\,\text{tool feed(mm·rev}^{-1}\text{)\_0.010} - 1.457\,\text{tool feed(mm·rev}^{-1}\text{)\_0.025} \\ & - 0.484\,\text{tool feed(mm·rev}^{-1}\text{)\_0.050} + 0.563\,\text{tool feed(mm·rev}^{-1}\text{)\_0.075} \\ & + 0.053\,\text{nose radius(mm)\_0.3} + 0.133\,\text{nose radius(mm)\_0.6} \\ & - 0.049\,\text{nose radius(mm)\_0.9} - 0.137\,\text{nose radius(mm)\_1.2.}\end{aligned} \tag{3}$$

The validation of a statistical model for the feed force response can be observed from the R^2 value of the model

there is a decrease in the cutting velocity, i.e. a decrease in the cutting speed possibilities (signals) increases the

Table 16: Model summary for the Taguchi analysis on the cutting force response

S	R^2	R^2 (adj)	R^2 (pred)
0.455190	98.94%	97.35%	92.47%

surface roughness [81,107–111]. Hence, the input setting of Level 4,80 m·min^{-1} cutting velocity (as maximum *S*/*N* ratio is –17.37), 0.100 mm·rev^{-1} (Level 4) feed rate (as maximum *S*/*N* ratio is –18.05), and 0.3 mm (Level 1) nose radius tool (as maximum *S*/*N* ratio is –18.25) gave a minimum surface roughness (Figure 16 and Table 17). The variability is found to be high in the cutting velocity input than in the tool feed and very low in the nose radius of the tool used [112–114]. Table 17 shows the results of the Taguchi analysis, which is the yield of *S*/*N* ratios.

Table 17: Taguchi analysis results for the observation of the surface roughness

Level	Cutting velocity (m·min^{-1})	Tool feed (mm·rev^{-1})	Nose radius (mm)
1	–19.08	–18.21	–18.25
2	–18.74	–18.66	–18.37
3	–18.17	–18.43	–18.39
4	–17.37	–18.05	–18.35
Delta	1.71	0.61	0.15
Rank	1	2	3

Table 17 ranks the process parameters based on their influence according to the delta value obtained in this statistical analysis. A higher delta value indicates a higher influence based on the delta value ranking of the process variable determined. Since the delta value for the cutting velocity is 1.71, which is greater than the data value of the tool feed and nose radius factors, the cutting velocity has the highest influence on the surface roughness during machining, ranking first (Rank 1). Accordingly, Rank 2 is for the tool feed (delta = 0.61), and Rank 3 is for the nose radius of the tool (delta = 0.15).

4.9 ANOVA results on the response of surface roughness

The residual plots for surface roughness observations are shown in Figure 17. The normal probability plot shows the quality of observations. No observations deviate much from the mean line, and residual errors in these observations are in the acceptable range. Hence, from Figure 17 and Table 18, it is evident that, except fifth observation, the remaining observations are acceptable as per the statistical verification by ANOVA.

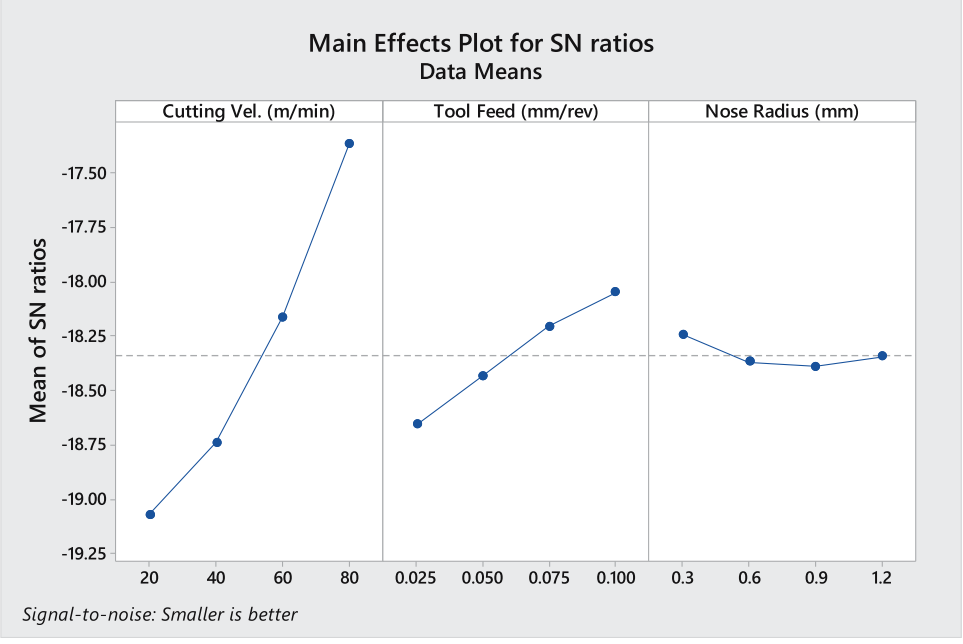

Figure 16: Main effect plots for the signal-to-noise ratio for the response observations of surface roughness during experiments with the proposed nanofluid.

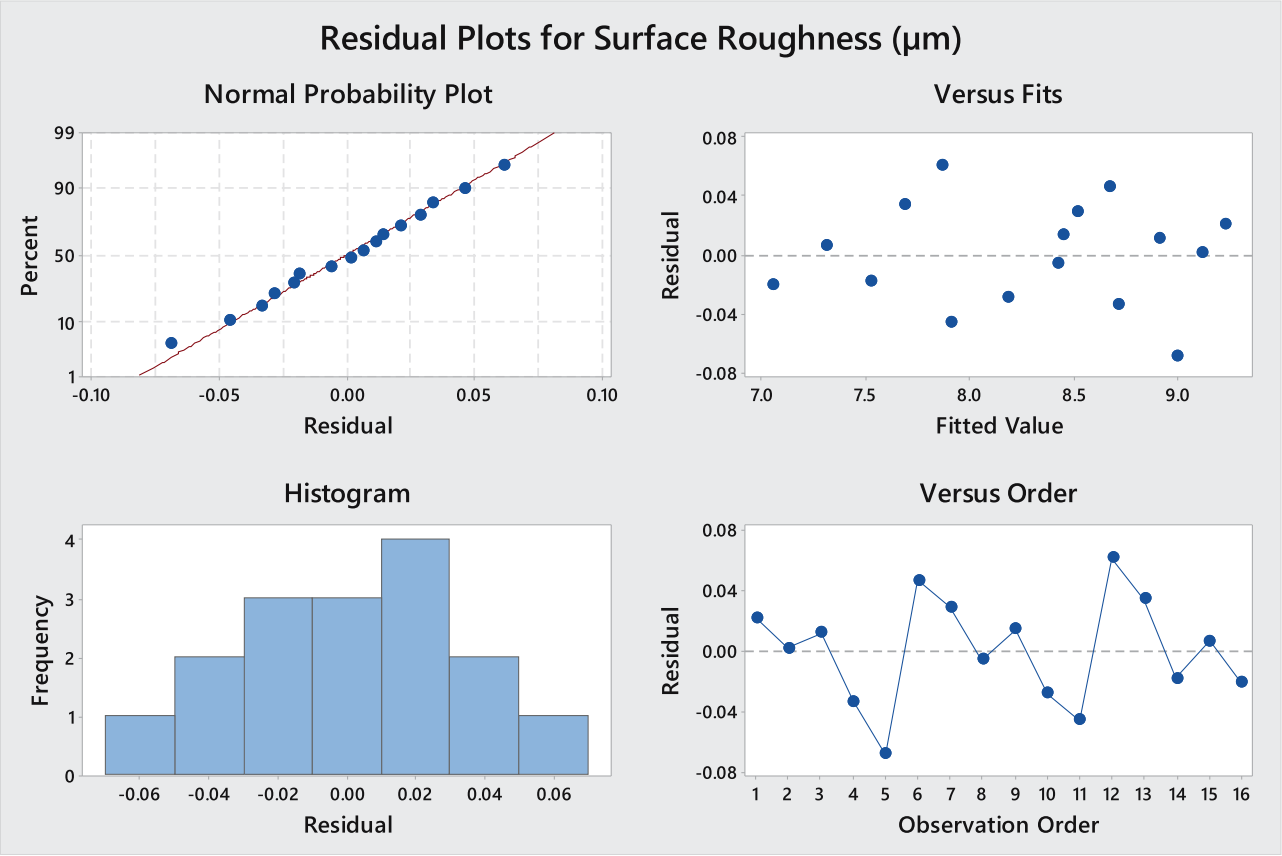

Figure 17: Residual plot for surface roughness observations.

Table 18: Fits and diagnostics for unusual observations of surface roughness

Observation	Surface roughness (μm)	Fit	Residual	Std residual	
5	8.9300	8.9987	−0.0687	−2.03	*R* is a large residual

Table 19 shows the results of the ANOVA on the response of surface roughness for the decision on the influence of factors. In this stage, one can take the decision on the factor level, based on the p-value. Here, a minimum p-value indicates more influence. The decision criteria are as follows: if $p < 0.05$, the factor is significantly influencing the measured response; $p > 0.1$ indicates an insignificant factor. From Taguchi analysis, it was observed that the surface roughness was of Rank 1 and the significant value was 0.001 (very low); similarly, $p = 0.001$ ($p < 0.05$) for the tool feed. But, in the case of the nose radius, $p = 0.090$ ($0.05 < p < 0.1$), and it did not influence considerably. Table 19 shows the results of ANOVA at a factor level decision making, which reveals that for obtaining the desired surface roughness, it is better to alter the cutting speed for the best response and alter the tool feed for fine tuning. The alternation tools with various nose radii should be avoided.

The table of coefficients is shown in Table 20, from which one can take a deep decision on the degree of influence of a factor at its level of input. Similar to Table 19, here, the p-value indicates the significance of the level of factors on the response. Table 20 recommends the use of a cutting tool with a nose radius of 0.3 mm for obtaining a significant response on the surface finish (lower surface roughness). The recommended range of cutting velocity is 20–60 $m \cdot min^{-1}$. Similarly, the tool feed from 0.10 to 0.025 $mm \cdot rev^{-1}$ will give appreciable results on the surface finish. Hence, the major contribution is the cutting velocity, and the tool feed rate inputs for the surface roughness and its interactive effects on the surface roughness on the job are depicted in Figure 18.

Table 19: Results of ANOVA for the analysis on the influence of factors

Source	DF	Adj SS	Adj MS	*F*-Value	*p*-Value
Cutting velocity ($m \cdot min^{-1}$)	3	5.89082	1.96361	642.49	0.000
Tool feed ($mm \cdot rev^{-1}$)	3	0.75682	0.25227	82.54	0.000
Nose radius (mm)	3	0.03202	0.01067	3.49	0.090
Error	6	0.01834	0.00306		
Total	15	6.69799			

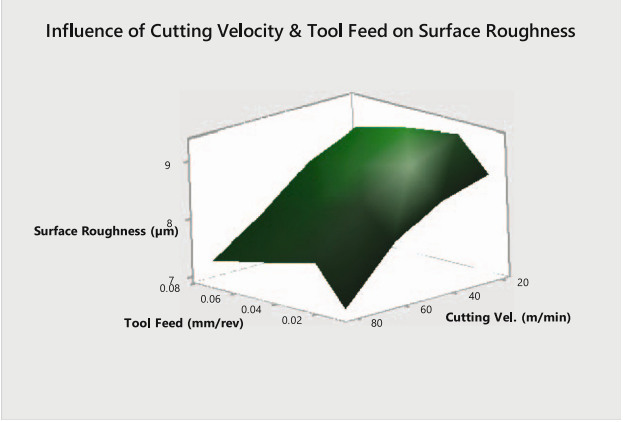

Figure 18: A 3D surface plot showing the relationship between the tool feed and cutting velocity in surface roughness response.

4.10 Regression equation

Table 20 mainly helps to form the mathematical model by generating the regression equation. From the mathematical model, one can interpret the values of untested combinations or predict the process parameter levels for the desired response. The regression model is given as follows:

R^2 value must be greater than 95% for a good model; in this case, the R^2 value is 99.73%. Hence, the model is acceptable. The R^2 value also confirms the reliability of the mathematical model (Eq. (3)) in the prediction of the response of surface roughness.

$$\begin{aligned}\text{Surface roughness}(\mu m) = {} & 8.2844 + 0.7081\ \text{cutting vel.}(m \cdot min^{-1})\_20 + 0.3706\ \text{cutting vel.}(m \cdot min^{-1})\_40 \\ & - 0.1844\ \text{cutting vel.}(m \cdot min^{-1})\_60 - 0.8944\ \text{cutting vel.}(m \cdot min^{-1})\_80 \\ & - 0.2694\ \text{tool feed}(mm \cdot rev^{-1})\_0.010 + 0.3056\ \text{tool feed}(mm \cdot rev^{-1})\_0.025 \\ & + 0.0881\ \text{tool feed}(mm \cdot rev^{-1})\_0.050 - 0.1244\ \text{tool feed}(mm \cdot rev^{-1})\_0.075 \\ & - 0.0694\ \text{nose radius}(mm)\_0.3 + 0.0381\ \text{nose radius}(mm)\_0.6 \\ & + 0.0406\ \text{nose radius}(mm)\_0.9 - 0.0094\ \text{nose radius}(mm)\_1.2.\end{aligned} \tag{4}$$

The validation of a statistical model for the surface roughness response can be observed from the R^2 value of the model summary (Table 21). The condition is that the

Table 20: Results of ANOVA on the response of surface roughness for the decision on the influence at the level of factors

Term	Coefficient	SE coefficient	*T*-Value	*p*-Value	VIF
Constant	8.2844	0.0138	599.41	0.000	
Cutting velocity ($m \cdot min^{-1}$)					
20	0.7081	0.0239	29.58	0.000	1.50
40	0.3706	0.0239	15.48	0.000	1.50
60	−0.1844	0.0239	−7.70	0.000	1.50
Tool feed ($mm \cdot rev^{-1}$)					
0.010	−0.2694	0.0239	−11.25	0.000	1.50
0.025	0.3056	0.0239	12.77	0.000	1.50
0.050	0.0881	0.0239	3.68	0.010	1.50
Nose radius (mm)					
0.3	−0.0694	0.0239	−2.90	0.027	1.50
0.6	0.0381	0.0239	1.59	0.162	1.50
0.9	0.0406	0.0239	1.70	0.141	1.50

4.11 Taguchi analysis on the cutting zone temperature

Taguchi analysis gives the degree of possibilities to achieve the objective function. Here, the objective is to minimize the cutting zone temperature (smaller is better in the signal-to-noise ratio). For this statistical model, the intervention group observations of cutting zone temperatures on 16 different experiments were used to optimize the proposed method. Figure 19 shows the main effect plots for signal-to-noise ratios for the response

Table 21: Model summary for the Taguchi analysis on the surface roughness response

S	R^2	R^2 (adj)	R^2 (pred)
0.0552834	99.73%	99.32%	98.05%

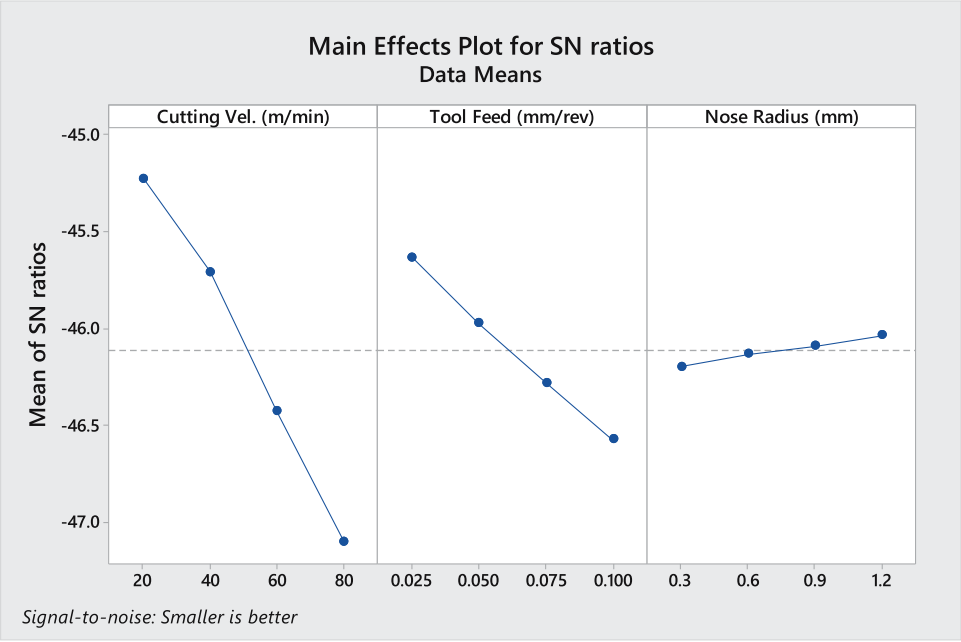

Figure 19: Main effect plots for signal-to-noise ratios for the response observations of the cutting zone temperature during experiments with the proposed nanofluid.

observations of the cutting zone temperature during experiments with the proposed nanofluid.

The mean line indicates large signals (possibilities towards the objective function of reducing the cutting zone temperature). The left-most graph for the cutting velocity shows an increase in the cutting zone temperature with an increase in the cutting velocity; in other words, a decrease of possibilities (signals) in minimizing the cutting zone temperature. Hence, the following input levels: level 1, 20 m·min^{-1} cutting velocity (as the maximum S/N ratio is −45.23); level 1, 0.025 mm·rev^{-1} feed rate (as maximum S/N ratio is −46.28); and level 4 of 0.3 mm nose radius tool (as maximum S/N ratio is −46.04) recorded a minimum cutting zone temperature (refer to Figure 19 and Table 22). The variability is found to be high in the cutting velocity input than the tool feed and very low in the nose radius of the tool used. Table 19 shows the results of the Taguchi analysis, which is the yield of S/N ratios.

The process parameters based on their influence according to the delta value obtained in this statistical analysis are shown in Table 22. The higher delta value indicates a higher influence based on the delta value ranking of the process variable. As the delta value for the cutting velocity is 5.58 and is greater than the delta values of the tool feed and nose radius factors, the cutting velocity is the no. 1 factor (Rank 1) and influences the cutting zone temperature while machining. Accordingly, Rank 2 is for the tool feed (delta = 1.41), and Rank 3 is for the nose radius of the tool.

Table 22: Taguchi analysis results for the observation of the cutting zone temperature

Level	Cutting velocity (m·min^{-1})	Tool feed (mm·rev^{-1})	Nose radius (mm)
1	−45.23	−46.28	−46.04
2	−45.71	−45.64	−46.13
3	−46.43	−45.97	−46.09
4	−47.10	−46.57	−46.20
Delta	1.88	0.94	0.16
Rank	1	2	3

4.12 ANOVA results on the response of the cutting zone temperature

The residual plots for cutting zone temperature observations are shown in Figure 20. The normal probability plot shows the quality of observations. The number of observations deviates from the mean line and the number of residual errors was observed in these observations. Hence, these observations are statistically acceptable.

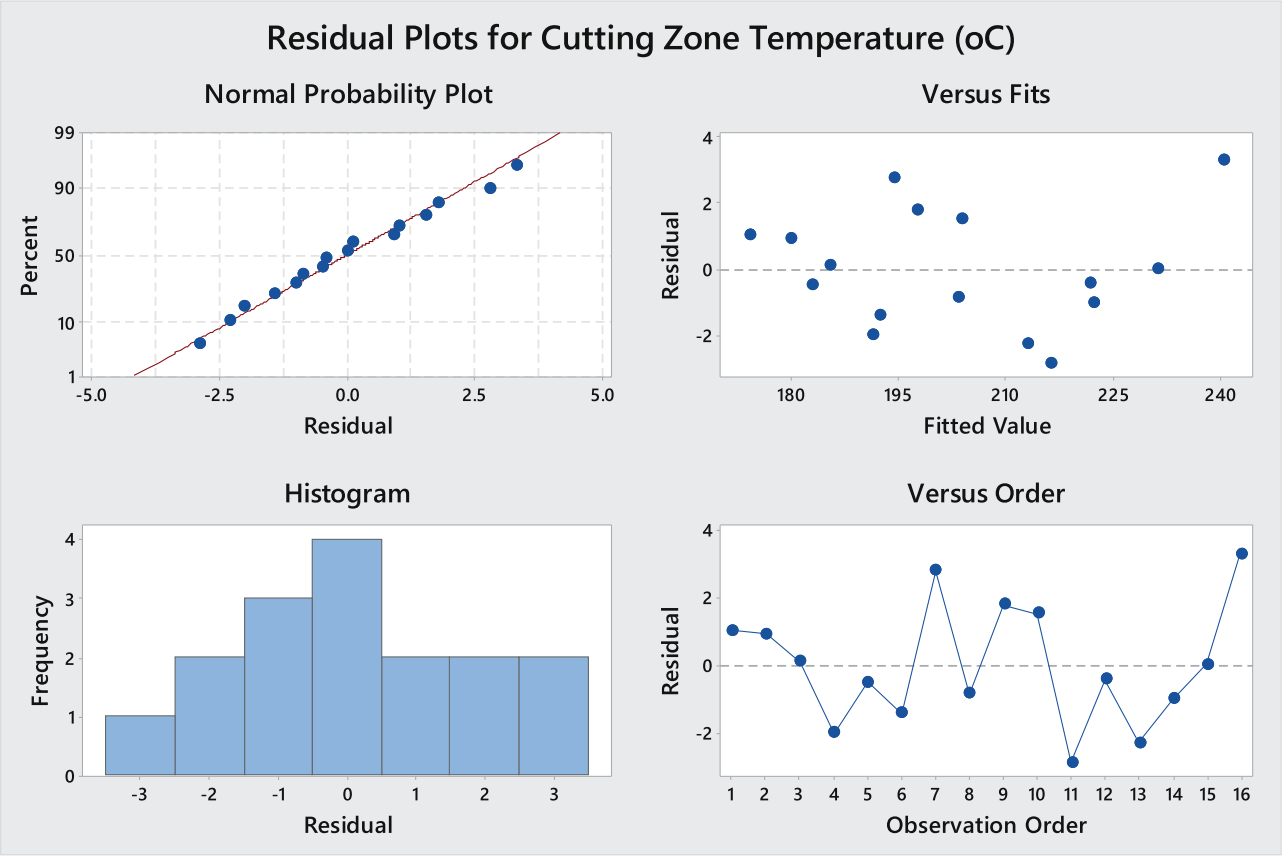

Figure 20: Residual plot for cutting zone temperature observations.

Table 23 shows the results of the ANOVA on the response of the cutting zone temperature for a decision on the influence of factors. In this stage, one can take a decision on the factor level based on the p-value. Here, a minimum p-value indicates more influence. The decision criteria are as follows: if $p < 0.05$, the factor is significantly influencing the measured response, and $p > 0.1$ indicates an insignificant factor. From Taguchi analysis, it was observed that the cutting zone temperature was of Rank 1 and the significant value was 0.001 (very low); similarly, $p = 0.001$ ($p < 0.05$) for the tool feed. But, in the case of the nose radius, $p = 0.156$ ($p > 0.1$), so it was found to be insignificant. Table 23 shows the results of ANOVA at the factor level decision making and it is concluded that all factors other than the nose radius of the tool are considered.

The table of coefficients is shown in Table 24, from which one can take a deep decision on the degree of the

Table 23: Results of ANOVA for the analysis on the influence of factors

Source	DF	Adj SS	Adj MS	*F*-Value	*p*-Value
Cutting velocity (m·min^{-1})	3	4512.80	1504.27	188.08	0.000
Tool feed (mm·rev^{-1})	3	1102.91	367.64	45.97	0.000
Nose radius (mm)	3	60.11	20.04	2.51	0.156
Error	6	47.99	8.00		
Total	15	5723.82			

Table 24: Results of ANOVA on the response of the cutting zone temperature for a decision on the influence at the level of factors

Term	Coefficient	SE coefficient	*T*-Value	*p*-Value	VIF
Constant	203.080	0.707	287.23	0.000	
Cutting velocity (m·min^{-1})					
20	−20.48	1.22	−16.72	0.000	1.50
40	−9.98	1.22	−8.15	0.000	1.50
60	6.71	1.22	5.48	0.002	1.50
Tool feed (mm·rev^{-1})					
0.010	11.07	1.22	9.04	0.000	1.50
0.025	−11.24	1.22	−9.18	0.000	1.50
0.050	−3.57	1.22	−2.92	0.027	1.50
Nose radius (mm)					
0.3	2.67	1.22	2.18	0.072	1.50
0.6	0.82	1.22	0.67	0.526	1.50
0.9	−0.98	1.22	−0.80	0.452	1.50

influence of the factor at its level of input. Similar to Table 23, here, the p-value indicates the significance of the level of factors on the response. Table 24 reflects the same decision as in Table 20 with some insights into the recommended range of input variation on the cutting velocity of 20–60 m·min^{-1} and the tool feed of 0.010–0.025 mm·rev^{-1}. Under unavoidable circumstances, the range may extend up to 0.050. The tool with a nose radius of 0.3 mm can be used for the minimum cutting zone temperature. Hence, the change in the tool radius is not recommended, and it is clear that there is a contribution from the cutting speed and tool feed, and the contribution from the nose radius of the tool used is negligible. The combined effects of the cutting speed and tool feed on the response of the cutting zone temperature are graphically depicted in Figure 21.

4.13 Regression equation

Table 24 mainly helps to form the mathematical model by generating the regression equation. From the mathematical model, one can interpret values of untested combinations or predict the process parameter levels for the desired response. The regression model is given as follows:

The validation of a statistical model for the cutting zone temperature response can be observed from the R^2 value of the model summary. Table 25 shows the model summary for the Taguchi analysis on the cutting zone temperature response. The condition is that the R^2 value must be greater than 95% for a good model. In this case, the R^2 value is 99.16%; hence, the model is acceptable. Apart from these, the R^2 values ensured the reliability of the mathematical model as shown in Eq. (4).

4.14 Taguchi analysis of the tool wear

Taguchi analysis gives the degree of possibilities to achieve the objective function. Here, the objective is to minimize the tool wear (the smaller the better).

For this statistical model, the intervention group observations of tool wear on 16 different experiments were used to optimize the proposed method. Figure 22 shows the main effect plots for signal-to-noise ratios for the response observations of tool wear during experiments with the proposed nanofluid. The mean line indicates large signals (possibilities towards the objective function of reducing the tool wear). The top leftmost

$$\begin{aligned}\text{Cutting zone temperature(°C)} = {} & 203.080 - 20.48\ \text{cutting vel.(m·min}^{-1}\text{)\_20} - 9.98\ \text{cutting vel.(m·min}^{-1}\text{)\_40} \\ & + 6.71\ \text{cutting vel.(m·min}^{-1}\text{)\_60} + 23.75\ \text{cutting vel.(m·min}^{-1}\text{)\_80} \\ & + 11.07\ \text{tool feed(mm·rev}^{-1}\text{)\_0.010} - 11.24\ \text{tool feed(mm·rev}^{-1}\text{)\_0.025} \\ & - 3.57\ \text{tool feed(mm·rev}^{-1}\text{)\_0.050} + 3.75\ \text{tool feed(mm·rev}^{-1}\text{)\_0.075} \\ & + 2.67\ \text{nose radius(mm)\_0.3} + 0.82\ \text{nose radius(mm)\_0.6} \\ & - 0.98\ \text{nose radius(mm)\_0.9} - 2.50\ \text{nose radius(mm)\_1.2}.\end{aligned} \tag{5}$$

graph for the cutting velocity shows an increase in tool wear with an increase in the cutting velocity; in other words, a decrease of possibilities (signals) when minimizing the tool wear. Hence, the input setting of Level 1, 20 m·min^{-1} (as the signal-to-noise ratio is 19.748) cutting velocity, 0.025 mm·rev^{-1} feed rate (as the signal-to-noise ratio is 13.219), and 0.3 mm nose radius of the tool (as the signal-to-noise ratio is 11.735) gave minimum tool wear (refer to Figure 22 and Table 26). The variability is found to be higher in the cutting velocity input than in

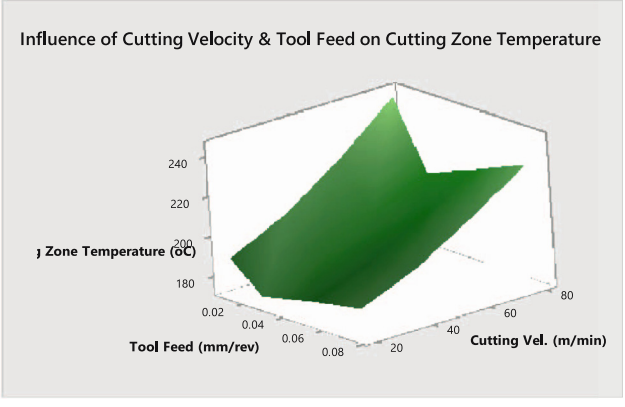

Figure 21: A 3D surface plot showing the relationship between the tool feed and cutting velocity in the cutting zone temperature response.

Table 25: Model summary for the Taguchi analysis on the cutting zone temperature response

S	R^2	R^2 (adj)	R^2 (pred)
2.82809	99.16%	97.90%	94.04%

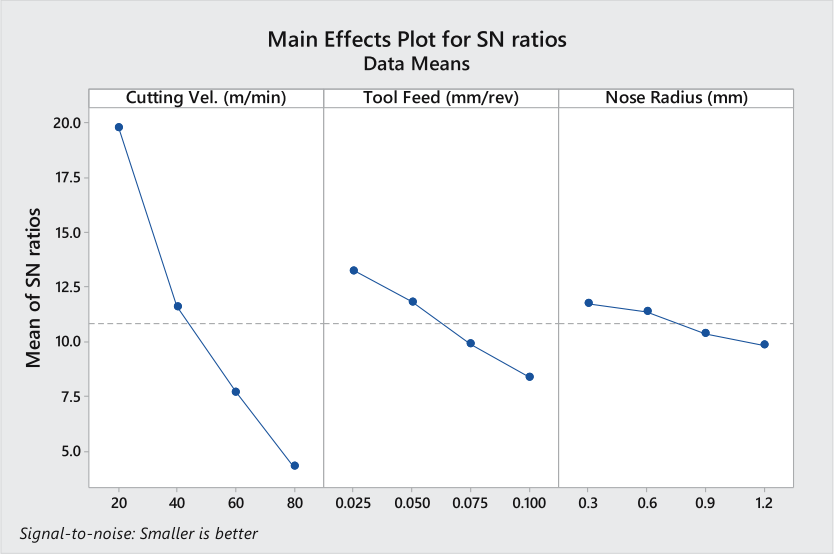

Figure 22: Main effect plots for the signal-to-noise ratio for the response observations of tool wear during experiments with the proposed nanofluid.

Table 26: Taguchi analysis results for the observation of the tool wear

Level	Cutting velocity ($m \cdot min^{-1}$)	Tool feed ($mm \cdot rev^{-1}$)	Nose radius (mm)
1	19.748	13.219	11.735
2	11.583	11.811	11.348
3	7.675	9.870	10.363
4	4.274	8.380	9.835
Delta	15.473	4.839	1.900
Rank	1	2	3

the tool feed and lower in the nose radius of the tool used. Table 26 shows the results of the Taguchi analysis, which was the yield of S/N ratios.

Figure 23 shows that all observations are statistically accepted as there is good nearness in the mean line in the residual plot. Table 27 illustrates the results of the ANOVA on the response of the tool wear for the decision on the influence of factors. In this stage, one can take a decision on the factor level based on the p-value. Here, the minimum p-value influences are more. The decision criteria are as follows: if $p < 0.05$, the factor is significantly influencing the measured response, and $p > 0.1$ indicates an insignificant factor. From Taguchi analysis, it was observed that the cutting velocity is of Rank 1 and its significant value is 0.001 (very low); similarly, $p = 0.004$ ($p < 0.05$) for the tool feed. But, in the case of nose radius, $p = 0.940$ ($p > 0.1$), so it was found to be insignificant. Table 27 shows the results of ANOVA at the factor level decision making and confirms that other than nose radius, all independent variables considered are significant and they can be used to control the process for rapid and fine-tuning for minimum tool wear. Figure 24 exhibits the 3D surface plot that shows the relationship between the tool feed and cutting velocity in the tool wear response.

The table of coefficients is shown in Table 28, from which one can take a deep decision on the degree of influence of the factor at its level of input. As in Table 27, the p-value indicates the significance of the level of factors on the response. Though Table 28 gives the same decision, it also gives some deep insights for controlling the tool wear: the cutting velocity should be varied from 20 to 60 $m \cdot min^{-1}$, the tool wear from 0.010 to 0.050 $mm \cdot rev^{-1}$, and 0.03 mm nose radius should be used than other three types of tools.

4.15 Regression equation

Table 28 mainly helps to form the mathematical model by generating the regression equation. From the mathematical model, one can interpret the values of untested combinations or predict the process parameter levels for the desired response. The regression model is given as follows:

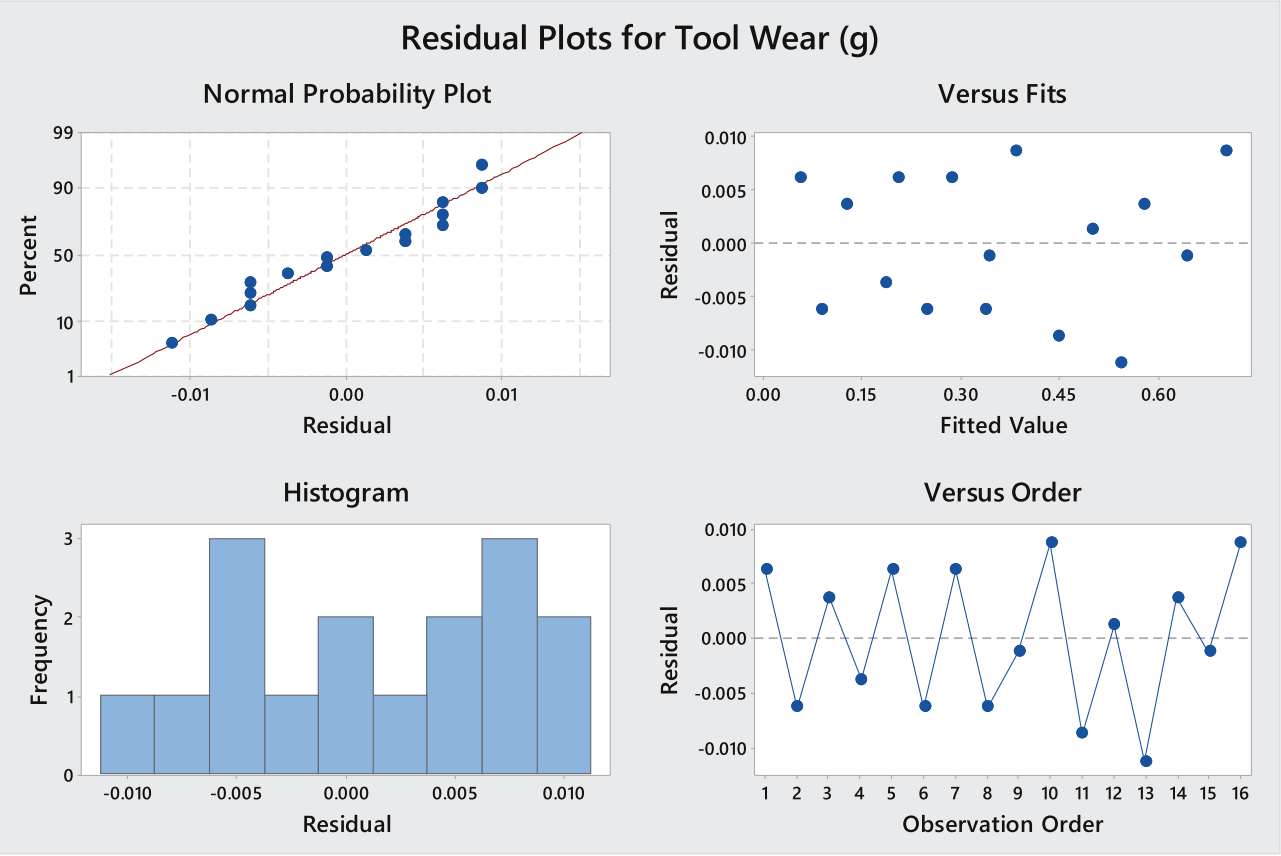

Figure 23: Residual plot for tool wear observations.

Table 27: Results of ANOVA for the analysis on the influence of factors on the tool wear

Source	DF	Adj SS	Adj MS	*F*-Value	*p*-Value
Cutting velocity (m·min^{-1})	3	0.551819	0.183940	1731.20	0.000
Tool feed (mm·rev^{-1})	3	0.047869	0.015956	150.18	0.000
Nose radius (mm)	3	0.000819	0.000273	2.57	0.150
Error	6	0.000637	0.000106		
Total	15	0.601144			

$$\begin{aligned}\text{Tool wear}(\text{mg}\cdot\text{h}^{-1}) = {} & 0.35312 - 0.24063\ \text{cutting vel.}(\text{m}\cdot\text{min}^{-1})\_20 - 0.08562\ \text{cutting vel.}(\text{m}\cdot\text{min}^{-1})\_40 \\ & + 0.06438\ \text{cutting vel.}(\text{m}\cdot\text{min}^{-1})60 + 0.26188\ \text{cutting vel.}(\text{m}\cdot\text{min}^{-1})\_80 \\ & + 0.07688\ \text{tool feed}(\text{mm}\cdot\text{rev}^{-1})\_0.010 - 0.06812\ \text{tool feed}(\text{mm}\cdot\text{rev}^{-1})\_0.025 \\ & - 0.03063\ \text{tool feed}(\text{mm}\cdot\text{rev}^{-1})\_0.050 + 0.02187\ \text{tool feed}(\text{mm}\cdot\text{rev}^{-1})\_0.075 \\ & + 0.00937\ \text{nose radius}(\text{mm})\_0.3 + 0.00437\ \text{nose radius}(\text{mm})\_0.6 \\ & - 0.00812\ \text{nose radius}(\text{mm})\_0.9 - 0.00562\ \text{nose radius}(\text{mm})\_1.2.\end{aligned} \tag{6}$$

The validation of the statistical model for the tool wear response can be observed from the R^2 value of the model summary. Table 29 furnishes the model summary for the Taguchi analysis on the tool wear response. The condition is that the R^2 value must be greater than 95% for a good model. In this case, the value of R^2 is 99.89%.

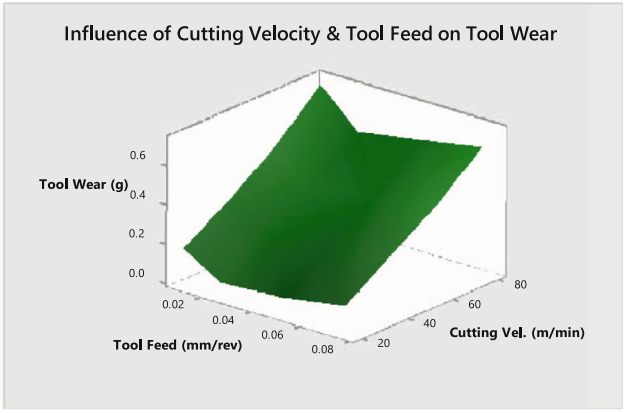

Figure 24: 3D surface plot showing a relationship between the tool feed and cutting velocity in the tool wear response.

Table 28: Results of ANOVA on the response of the tool wear for a decision on the influence at the level of factors

Term	Coefficient	SE coefficient	*T*-Value	*p*-Value	VIF
Constant	0.35312	0.00258	137.03	0.000	
Cutting velocity (m·min^{-1})					
20	−0.24063	0.00446	−53.91	0.000	1.50
40	−0.08562	0.00446	−19.18	0.000	1.50
60	0.06438	0.00446	14.42	0.000	1.50
Tool feed (mm·rev^{-1})					
0.010	0.07688	0.00446	17.22	0.000	1.50
0.025	−0.06812	0.00446	−15.26	0.000	1.50
0.050	−0.03063	0.00446	−6.86	0.000	1.50
Nose radius (mm)					
0.3	0.00937	0.00446	2.10	0.080	1.50
0.6	0.00437	0.00446	0.98	0.365	1.50
0.9	−0.00812	0.00446	−1.82	0.119	1.50

Table 29: Model summary for the Taguchi analysis on the tool wear response

S	R^2	R^2 (adj)	R^2 (pred)
0.0103078	99.89%	99.73%	99.25%

Hence, the model is acceptable. Moreover, the R^2 value also confirmed the reliability and accuracy of the prediction model (Eq. (5)).

Hence, the proposed manufacturing process outperformed other methods. The machinability includes a reduction in all five aspects: the cutting force, feed force, cutting zone temperature, surface roughness, and tool wear [115,116]. The limitation of this study is that the influence of specially coated tool inserts was not included in the examinations. The harder tool suffers from less tool wear, and the machinability of the surface roughness will be reduced further. Another limitation is that too small implants could not be machined by using this processing method. The future scope shall include process variables that do not affect the quality of the implant thermally and chemically to improve the surface quality. The tested samples are exhibited in Figure 25.

4.16 Scanning electron microscopy examination

Though we have considered the wear rate here, the scanning electron microscopy examination was carried out to observe the nature of the tool wear. The tool wear was observed at a low cutting speed (left side image in Figure 26) and high cutting speed. As the work material is softer compared to the tool material, the shape changes were not significant. But little flank wear was observed.

Venkatesan *et al.* [52] utilized fresh coconut oil for preparing the nanofluid by mixing 0.25 wt% Al_2O_3 nanoparticles for machining Inconel 617 by CNC turning. The process parameters, such as cutting speed and feed rate, were optimized based on their impact on cutting force, surface roughness, and tool wear. For their statistical models, the R^2 value was 82.27% for the surface roughness, 78.04% for the cutting force, and 72.31% for the tool wear, and no confirmation experimentation was reported. Yücel *et al.* [35] prepared the nanofluid by enhancing the commercial conventional nanofluid by mixing 0.6 vol% of MoS_2 for machining the aluminium alloy 2024 T3. The temperature was reduced by 21°C in the MQL mode using a commercial fluid than dry machining and reduced by 43°C using MoS_2-based nanofluid in the MQL mode. The surface roughness was reduced by 0.432 µm in the MQL mode using a commercial fluid than dry machining and reduced by 0.728 µm using a MoS_2-based nanofluid in the MQL mode. Şirin and Kivak [40] utilized a concentration of 0.25 vol% for each kind of nanoparticle and maintained a total concentration of 50 vol%. The graphite, MoS_2, and boron nitride nanoparticles were used in all three possible combinations for preparing the hybrid nanoparticle mixed nanofluid in MQL; for machining the graphite and boron nitride hybrid nanoparticles based nanofluid in MQL, the cutting force was reduced by 10.22 and 3.77%, the peak temperature by 6.92 and 10.78%, and the surface roughness by 14.95 and 8.21%, whereas tool life value improved by 36.17 and 6.08% compared to graphite/MoS_2 and boron nitride.

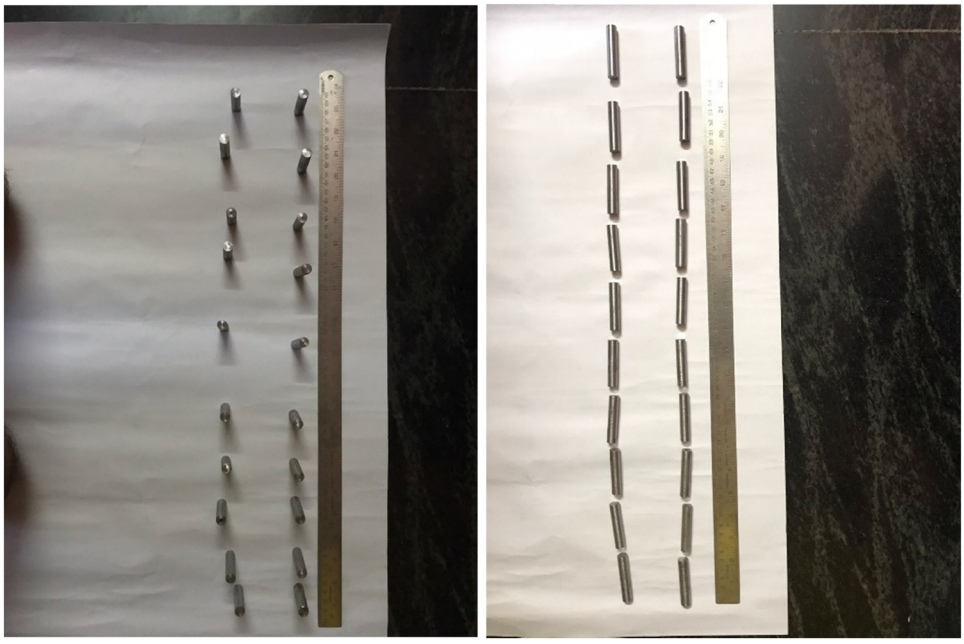

Figure 25: Machinability investigated and tested samples.

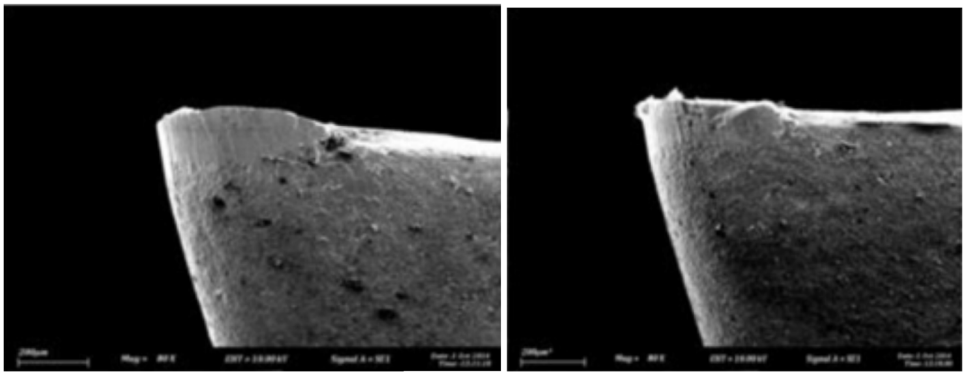

Figure 26: SEM images of the tool after machining at low speed (left) and high speed (right).

This research utilized a low concentration of MoS_2 nanoparticles (0.3 wt%) with waste oil (used coconut oil) as a base fluid to prepare the nanofluid for machining biocompatible magnesium implants for biomedical applications under flood cooling conditions. The nanofluid can be reused multiple times in flood cooling, whereas it cannot be reused under MQL conditions. The prepared nanofluid is not harmful to humans as it has edible oil as a base fluid and flood cooling generates less mist than MQL, so it exerts great care for the operator and other workers in the shop. It is a biodegradable coolant with no harm to environmental pollution. The experimental results were compared with the results using a commercial cutting fluid. This research contains two phases that first compared the performance of the proposed nanofluid with a conventional commercial nanofluid in terms of reduction of the cutting force, feed force, cutting zone temperature, tool wear, and surface roughness. Then, the process parameters were optimized for the best-performing method (the proposed nanofluid with a conventional commercial nanofluid under flood cooling conditions).

This research considered average performance under all cutting conditions for comparison for the recommendation. This improved the reliability of the decision. The proposed nanofluid averagely reduced the cutting force by 68.232 N, the feed force by 34.180 N, the surface roughness by 0.118908 μm, and the tool wear by 0.39938 $mg{\cdot}h^{-1}$

compared to the conventional commercial cutting fluid. The cost of cutting is a considerable expenditure in metal machining processes. The regression model was developed based on the experimental results of the cutting force, feed force, cutting zone temperature, surface roughness, and tool wear and presented. The accuracy of developed regression equations for predicting the responses was confirmed as follows. The statistical models were verified with ANOVA. The R^2 values were based on proposed nanofluid observations under flood cooling conditions: 99.22% for the cutting force model, 98.94% for the feed force model, 99.73% for the surface roughness model, 99.16% for the cutting zone temperature model, and 99.89% for the tool wear model. As the obtained R^2 values are greater than 95%, it indicates that there is good agreement between the predicted responses with the use of the regression model and experimental results.

From the Taguchi analysis, it was observed that the nose radius of the tool does not influence the responses significantly, and the best values were obtained at 0.3 mm nose radius. The other two factors were significantly influenced as they possess very low p values [36]. Hence, the cutting speed and tool feed were considered for surface plots. For better presentation, the 3D surface plot was used to reveal the relationship between the above-said variables for responses of cutting force, feed force, cutting zone temperature, tool wear, and surface roughness [37]. The highly influenced parameters were decided based on the experimental results based on Taguchi analysis results [38]. The ranking was based on the influence of the factor on the response. The ranking of variables is shown in Tables 8 and 12 and 17 and 22 and and 26 for the cutting force, feed force, surface roughness, cutting zone temperature, and tool wear responses. The higher delta values indicate a high influence of factors for the concerned response. Venkatesan *et al.* [52] recommended Taguchi analysis for optimizing the process parameters effectively. They also recommended ANOVA for obtaining the significance of influencing process parameters [39]. The process parameters were optimized with the help of the Taguchi analysis for all five responses and presented [37]. It was found that the cutting velocity and tool feed parameters were highly influenced in all five responses significantly [38]. However, the nose radius of 0.3 mm seems to be the best, as inferred from the Taguchi analysis.

The statistical evaluation showed the significance values $p = 0.001$, $p = 0.023$, $p = 0.001$, $p = 0.045$, and $p = 0.028$ for observations of the cutting force, feed force, surface roughness, cutting zone temperature, and tool wear by using the proposed nanofluid and conventional commercial coolant. All these p-values were less than 0.05. The comparison performed in this work was done on average values.

5 Conclusions

This work demonstrates the low-cost, high-performance cutting fluid (nanofluid) developed from the multiple times used coconut oil (waste) mixed with MoS_2 nanoparticles. The concentration is optimized by the trial and error method. The prepared nanofluid was characterized well before experimentation. The prepared nanofluid was tested experimentally and compared with the performance of the conventional commercial coolant. These observations are statistically significant and confirm that these observations can be accepted. Hence, the use of the proposed nanofluid in place of a conventional commercial coolant averagely reduced the cutting force by 68.23167 N, the feed force by 34.180 N (as the nanofluid supplied sufficient lubrication action for minimizing the forces and absorbing some vibrational effects by maintaining a layer in between the tool and workpiece), the cutting zone temperature by 60.435°C (due to nanofluid lubrication for easy shearing of the material with a hard tool in supplement with cooling), the surface roughness by 0.118908 µm (the lubricated shearing allowed one to make fine cutting and prevented fast wear of sharp tool edges), and the tool wear by 0.39938 $mg{\cdot}h^{-1}$ (the lubricated cutting reduced the tool force and permitted the operation to occur smoothly). The proposed method (use of a nanofluid under flood cooling) outperformed other methods. To generalize these outcomes, the process parameters were optimized for using the proposed method for obtaining the best performance. The optimal conditions were presented, and mathematical models (regression equation) were developed to predict the responses. The mathematical models' accuracies were verified with R^2 values. The R^2 values confirmed that the predictions of the developed models have good agreement with experimental results, and the model is accurate. The proposed nano coolant was prepared with extreme care for high-temperature application by concentrating MoS_2 in used coconut oil without the water content by understanding the physical phenomenon of cutting processes. The expected outcomes are given in the experimental results. Within the limitation of this study, the coolant was tested for machining magnesium samples. In the future, this coolant will be inspected with the machining of precision materials, in CNC milling, CNC grinding, conventional milling, deep drilling processes, etc.

Funding information: The authors state no funding involved.

Author contributions: Conceptualization: RS, TS, VV, SR, SS; formal analysis: RS, TS, VV, SR, SS; investigation: RS, TS, VV, SR, SS; writing – original draft preparation: RS, TS, VV, SR, SS; writing – review and editing: SS, CL, YZ, KS, SME; supervision: SS, CL, YZ, KS, SME; project administration: SS, CL, YZ, KS, SME; funding acquisition: SS, SME. All authors have accepted responsibility for the entire content of this article and approved its submission.

Conflict of interest: The authors state no conflict of interest.

References

[1] Tsakiris, V., C. Tardei, and F. M. Clicinschi. Biodegradable Mg alloys for orthopedic implants – A review. *Journal of Magnesium and Alloys*, Vol. 9, No. 6, 2021, pp. 1884–1905.

[2] Bishop, J. A., A. A. Palanca, M. J. Bellino, and D. W. Lowenberg. Assessment of compromised fracture healing. *JAAOS-Journal of the American Academy of Orthopaedic Surgeons*, Vol. 20, No. 5, 2012, pp. 273–282.

[3] Kamrani, S. and C. Fleck. Biodegradable magnesium alloys as temporary orthopaedic implants: a review. *Biometals*, Vol. 32, No. 2, 2019, pp. 185–193.

[4] The American Foundry Society Technical Dept Magnesium Alloys, The American Foundry Society, Schaumburg, IL; 2006.

[5] Xu, T., Y. Yang, X. Peng, J. Song, and F. Pan. Overview of advancement and development trend on magnesium alloy. *Journal of Magnesium and Alloys*, Vol. 7, No. 3, 2019, pp. 536–544.

[6] Husak, Y., J. Michalska, O. Oleshko, V. Korniienko, K. Grundsteins, B. Dryhval, et al. Bioactivity performance of pure mg after plasma electrolytic oxidation in silicate-based solutions. *Molecules*, Vol. 26, No. 7, 2021, id. 2094.

[7] Willbold, E., X. Gu, D. Albert, K. Kalla, K. Bobe, M. Brauneis, C. Janning, et al. Effect of the addition of low rare earth elements neodymium, cerium) on the biodegradation and biocompatibility of magnesium. *Acta Biomaterialia*, Vol. 11, 2015, pp. 554–562.

[8] Williams, D. New interests in magnesium. *Medical Device Technology*, Vol. 17, No. 3, 2006, pp. 9–10.

[9] Avedesian, M. M. and H. Baker, editors, *A. S.M. specialty handbook: magnesium and magnesium alloys*, A.S.M. international, USA, 1999.

[10] Housh, S., B. Mikucki, and A. Stevenson. *Properties of magnesium alloys*, ASM International, USA, 1990.

[11] Xu, L., E. Zhang, D. Yin, S. Zeng, and K. Yang. *In vitro* corrosion behaviour of Mg alloys in a phosphate buffered solution for bone implant application. *Journal of Materials Science: Materials in Medicine*, Vol. 19, No. 3, 2008, pp. 1017–1025.

[12] Staiger, M. P., A. M. Pietak, J. Huadmai, and G. Dias. Magnesium and its alloys as orthopedic biomaterials: a review. *Biomaterials*, Vol. 27, No. 9, 2006, pp. 1728–1734.

[13] Chen, J., L. Tan, and K. Yang. Recent advances on the development of biodegradable magnesium alloys: a review. *Materials Technology*, Vol. 31, No. 12, 2016, pp. 681–688.

[14] López, H. Y., D. A. Cortés-Hernández, S. Escobedo, and D. Mantovani. *In vitro* bioactivity assessment of metallic magnesium. In *Key Engineering Materials*, Trans Tech Publications Ltd, Switzerland, Vol. 309, 2006, pp. 453–456.

[15] Popescu, I. N., R. Vidu, and V. Bratu. Porous metallic biomaterials processing part 1: compaction, sintering behavior, properties and medical applications. *Scientific Bulletin of Valahia University Materials & Mechanics*, Vol. 15, No. 13, 2017, pp. 28–40.

[16] Lévesque, J., H. Hermawan, D. Dubé, and D. Mantovani. Design of a pseudo-physiological test bench specific to the development of biodegradable metallic Biomaterials. *Acta Biomaterialia*, Vol. 4, No. 2, 2008, pp. 284–295.

[17] Gupta, A. P. and V. Kumar. New emerging trends in synthetic biodegradable polymers–Polylactide: A critique. *European Polymer Journal*, Vol. 43, No. 10, 2007, pp. 4053–4074.

[18] Hermawan, H. Biodegradable metals: state of the art. *Biodegradable Metals*, Springer, Berlin, Heidelberg, 2012, pp. 13–22.

[19] Hermawan, H. Updates on the research and development of absorbable metals for biomedical applications. *Progress in Biomaterials*, Vol. 7, No. 2, 2018, pp. 93–110.

[20] Chohan, J. S., N. Mittal, R. Kumar, S. Singh, S. Sharma, S. P. Dwivedi, et al. Optimization of F.F.F. process parameters by naked mole-rat algorithms with enhanced exploration and exploitation capabilities. *Polymers*, Vol. 13, No. 11, 2021, id. 1702.

[21] Ilyas, R. A., S. M. Sapuan, M. R. Asyraf, D. A. Dayana, J. J. Amelia, and M. S. Rani. Polymer composites filled with metal derivatives: a review of flame retardants. *Polymers*, Vol. 13, No. 11, 2021, id. 1701.

[22] Chohan, J. S., N. Mittal, R. Kumar, S. Singh, S. Sharma, J. Singh, et al. Mechanical strength enhancement of 3D printed acrylonitrile butadiene styrene polymer components using neural network optimization algorithm. *Polymers*, Vol. 12, No. 10, 2020, id. 2250.

[23] Singh, Y., J. Singh, S. Sharma, V. Aggarwal, and C. I. Pruncu. Multi-objective optimization of kerf-taper and surface-roughness quality characteristics for cutting-operation on coir and carbon fibre reinforced epoxy hybrid polymeric composites during CO2-pulsed laser-cutting using R. S.M. *Lasers in Manufacturing and Materials Processing*, Vol. 8, No. 2, 2021, pp. 157–182.

[24] Sharma, S., J. Singh, H. Kumar, A. Sharma, V. Aggarwal, A. S. Gill, et al. Utilization of rapid prototyping technology for the fabrication of an orthopedic shoe inserts for foot pain reprieve using thermo-softening viscoelastic polymers: a novel experimental approach. *Measurement and Control*, Vol. 53, No. 3–4, 2020, pp. 519–530.

[25] Singh, Y., J. Singh, S. Sharma, A. Sharma, and J. S. Chohan. Process parameter optimization in laser cutting of coir fiber

reinforced epoxy composite—a review. *Materials Today: Proceedings*, 2021, pp. 4738–4744, in press.
[26] Chohan, J. S., R. Kumar, T. B. Singh, S. Singh, S. Sharma, J. Singh, et al. Taguchi *S/N* and T. O.P. S.I. S. based optimization of fused deposition modelling and vapor finishing process for manufacturing of A. B.S. plastic parts. *Materials*, Vol. 13, No. 22, 2020, id. 5176.
[27] Arun, K. and G. R. Devi. Comparison of novel TiN coated and uncoated carbide tool in C. N.C. green machining of AISI H13 to minimize tool wear. *Materials Today: Proceedings*, Vol. 69, 2022, pp. 827–831. https://www.sciencedirect.com/science/article/pii/S2214785322048945.
[28] Jagadeesan, S. and G. R. Devi. Comparison of novel TiN coated and uncoated carbide tool in C. N.C. dry turning of EN31 to analyze chip profile. *Materials Today: Proceedings*, Vol. 69, 2022, pp. 816–820. https://www.sciencedirect.com/science/article/pii/S221478532204857X.
[29] Wang, Y., A. Murga, Z. Long, S. J. Yoo, and K. Ito. Experimental study of oil mist characteristics generated from minimum quantity lubrication and flood cooling. *Energy and Built Environment*, Vol. 2, No. 1, 2021, pp. 45–55. https://www.sciencedirect.com/science/article/pii/S2666123320300428.
[30] Singh, R. and V. Sharma. Experimental investigations into sustainable machining of Hastelloy C-276 under different lubricating strategies. *Journal of Manufacturing Processes*, Vol. 75, 2022, pp. 138–153. https://www.sciencedirect.com/science/article/pii/S1526612522000032.
[31] Rajaguru, J. and N. Arunachalam. A comprehensive investigation on the effect of flood and MQL coolant on the machinability and stress corrosion cracking of super duplex stainless steel. *Journal of Materials Processing Technology*, Vol. 276, 2020, id. 116417. https://www.sciencedirect.com/science/article/pii/S0924013619303899.
[32] Khatri, A. and M. P. Jahan. Investigating tool wear mechanisms in machining of Ti-6Al-4V in flood coolant, dry and MQL conditions. *Procedia Manufacturing*, Vol. 26, 2018, pp. 434–445. https://www.sciencedirect.com/science/article/pii/S2351978918307212.
[33] Peng, R., J. Tong, L. Zhao, X. Tang, X. Peng, and X. He. Molecular dynamics study on the adsorption synergy of M. W.C. N.T.s/MoS_2 nanofluids and its influence of internal-cooling grinding surface integrity. *Applied Surface Science*, Vol. 563, 2021, id. 150312. https://www.sciencedirect.com/science/article/pii/S0169433221013878.
[34] Köhn, C., R. Arafat, A. Jean-Fulcrand, T. Abraham, C. Herrmann, and G. Garnweitner. Surface interactions of SiO2-nanofluids with 100Cr6-steel during machining. *Procedia CIRP*, Vol. 108, 2022, pp. 13–18. https://www.sciencedirect.com/science/article/pii/S2212827122004826.
[35] Yücel, A., Ç. V. Yıldırım, M. Sarıkaya, Ş. Şirin, T. Kıvak, M. K. Gupta, et al. Influence of MoS_2 based nanofluid-MQL on tribological and machining characteristics in turning of AA 2024 T3 aluminum alloy. *Journal of Materials Research and Technology*, Vol. 15, 2021, pp. 1688–1704. https://www.sciencedirect.com/science/article/pii/S2238785421009881.
[36] Ibrahim, A. M., M. A. Omer, S. R. Das, W. Li, M. S. Alsoufi, and A. Elsheikh. Evaluating the effect of minimum quantity lubrication during hard turning of AISI D3 steel using vegetable oil enriched with nano-additives. *Alexandria Engineering Journal*, Vol. 61, No. 12, 2022, pp. 10925–10938.
[37] Mahapatra, S., A. Das, P. C. Jena, S. R. Das. Turning of hardened AISI H13 steel with recently developed S3P-AlTiSiN coated carbide tool using MWCNT mixed nanofluid under minimum quantity lubrication. *Proceedings of the Institution of Mechanical Engineers, Part C: Journal of Mechanical Engineering Science*, Vol. 237, 2022, pp. 843–864.
[38] Dash, L., S. Padhan, and S. R. Das. Design optimization for analysis of surface integrity and chip morphology in hard turning. *Structural Engineering and Mechanics*, Vol. 76, No. 5, December 2020, pp. 561–578.
[39] Das, A., S. Patel, B. Biswal, and S. Das. Performance evaluation of aluminium oxide nanoparticles in cutting fluid with minimum quantity lubrication technique in turning of hardened AISI 4340 alloy steel. *Scientia Iranica*, Vol. 27, No. 6, 2020, pp. 2838–2852.
[40] Şirin, Ş. and T. Kıvak. Effects of hybrid nanofluids on machining performance in MQL-milling of Inconel X-750 superalloy. *Journal of Manufacturing Processes*, Vol. 70, 2021, pp. 163–176. https://www.sciencedirect.com/science/article/pii/S1526612521006150.
[41] Esfe, M. H., M. Bahiraei, and A. Mir. Application of conventional and hybrid nanofluids in different machining processes: A critical review. *Advances in Colloid and Interface Science*, Vol. 282, 2020, id. 102199. https://www.sciencedirect.com/science/article/pii/S0001868620301421.
[42] Yıldırım, Ç. V., Ş. Şirin, T. Kıvak, and M. Sarıkaya. A comparative study on the tribological behavior of mono&proportional hybrid nanofluids for sustainable turning of AISI 420 hardened steel with cermet tools. *Journal of Manufacturing Processes*, Vol. 73, 2022, pp. 695–714. https://www.sciencedirect.com/science/article/pii/S1526612521008513.
[43] Liu, H., Y. Ayed, H. Birembaux, F. Rossi, and G. Poulachon. Impacts of flank wear and cooling strategies on evolutions of built-up edges, diffusion wear and cutting forces in Ti6Al4V machining. *Tribology International*, Vol. 171, 2022, id. 107537 ISSN 0301-679X. https://www.sciencedirect.com/science/article/pii/S0301679X22001104.
[44] Hegab, H., A. Damir, and H. Attia. Sustainable machining of Ti-6Al-4V using cryogenic cooling: an optimized approach. *Procedia CIRP*, Vol. 101, 2021, pp. 346–349. https://www.sciencedirect.com/science/article/pii/S2212827121007277.
[45] Wu, G., G. Li, W. Pan, I. Raja, X. Wang, and S. Ding. Experimental investigation of eco-friendly cryogenic minimum quantity lubrication (C.MQL) strategy in machining of Ti–6Al–4V thin-wall part. *Journal of Cleaner Production*, Vol. 357, 2022, id. 131993. https://www.sciencedirect.com/science/article/pii/S0959652622016018.
[46] Ross, N. S., M. Mia, S. Anwar, G. Manimaran, M. Saleh, and S. Ahmad. A hybrid approach of cooling lubrication for sustainable and optimized machining of Ni-based industrial alloy. *Journal of Cleaner Production*, Vol. 321, 2021, id. 128987. https://www.sciencedirect.com/science/article/pii/S0959652621031784.
[47] Arul, K., V. Mohanavel, S. Raj Kumar, T. Maridurai, K. Magesh Kumar, and M. Ravichandran. Investigation of machining

attributes on machining of alloys under nanofluid MQL environment: A review. *Materials Today: Proceedings*, Vol. 59, No. Part 2, 2022, pp. 1312–1318. https://www.sciencedirect.com/science/article/pii/S2214785321075465.

[48] Dibyajyoti Panda, K. K. and N. Dalai. Performance of minimum quantity lubrication (MQL) and its effect on Dry Machining with the addition of Nano-particle with the biodegradable base fluids: A review. *Materials Today: Proceedings*, Vol. 56, No. Part 3, 2022, pp. 1298–1301. https://www.sciencedirect.com/science/article/pii/S2214785321072783.

[49] Race, A., I. Zwierzak, J. Secker, J. Walsh, J. Carrell, T. Slatter, et al. Environmentally sustainable cooling strategies in milling of SA516: Effects on surface integrity of dry, flood and MQL machining. *Journal of Cleaner Production*, Vol. 288, 2021, id. 125580. https://www.sciencedirect.com/science/article/pii/S0959652620356262.

[50] Singh, S., J. S. Chohan, and G. Singh. Experimental investigation into machining of hastelloy C-276 during different cooling environments. *Materials Today: Proceedings*, Vol. 48, No. Part 5, 2022, pp. 1123–1129. https://www.sciencedirect.com/science/article/pii/S2214785321055036.

[51] Chinchanikar, S., S. S. Kore, and P. Hujare. A review on nanofluids in minimum quantity lubrication machining. *Journal of Manufacturing Processes*, Vol. 68, No. Part A, 2021, pp. 56–70. https://www.sciencedirect.com/science/article/pii/S1526612521003583.

[52] Venkatesan, K., A. Tom Mathew, S. Devendiran, N. M. Ghazaly, S. Sanjith, and R. Raghul. Machinability study and multi-response optimization of cutting force, Surface roughness and tool wear on C. N.C. turned Inconel 617 superalloy using Al2O3 Nanofluids in Coconut oil. *Procedia Manufacturing*, Vol. 30, 2019, pp. 396–403. https://www.sciencedirect.com/science/article/pii/S235197891930085X.

[53] Hussain, Z. Comparative study on improving the ball mill process parameters influencing on the synthesis of ultrafine silica sand: a Taguchi coupled optimization technique. *International Journal of Precision Engineering and Manufacturing*, Vol. 22, 2021, pp. 679–688.

[54] Naqiuddin, N. H., L. H. Saw, M. C. Yew, F. Yusof, H. M. Poon, Z. Cai, et al. Numerical investigation for optimizing segmented micro-channel heat sink by Taguchi-Grey method. *Applied Energy*, Vol. 222, 2018, pp. 437–450.

[55] Bowen, P. K., J. Drelich, and J. Goldman. Zinc exhibits ideal physiological corrosion behavior for bioabsorbable stents. *Adv Mater*, Vol. 25, No. 18, 2013 May, pp. 2577–2582. Epub 2013 Mar 14. P.M.I.D.: 23495090.

[56] Purnama, A., H. Hermawan, J. Couet, and D. Mantovani. Assessing the biocompatibility of degradable metallic materials: state-of-the-art and focus on the potential of genetic regulation. *Acta Biomater*, Vol. 6, No. 5, 2010 May, pp. 1800–1807. Epub 2010 Feb 20. P.M.I.D.: 20176149.

[57] Shunmugesh, K., K. Panneerselvam, and M. Pramod. Optimization of CNC turning parameters with carbide tool for surface roughness analysis using Taguchianalysis. *Research Journal of Engineering Sciences*, Vol. 3, No. 6, 2014, pp. 1–7.

[58] Danish, M., T. L. Ginta, A. M. Rani, D. Carou, J. P. Davim, S. Rubaiee, et al. Investigation of surface integrity induced on AZ31C magnesium alloy turned under cryogenic and dry conditions. *Procedia Manufacturing*, Vol. 41, 2019, pp. 476–483.

[59] Eker, B., B. Ekici, M. Kurt, and B. Bakur. Sustainable machining of the magnesium alloy materials in the CNC lathe machine and optimization of the cutting conditions. *Mechanika*, Vol. 3, 2014, pp. 310–316.

[60] Machado, P. A., J. M. do Vale Quaresma, A. Garcia, and C. A. dos Santos. Investigation on machinability in turning of as-cast and T6 heat-treated Al-(3, 7, 12%) Si-0.6% Mg alloys. *Journal of Manufacturing Processes*, Vol. 75, 2022, pp. 514–526.

[61] Saravanakumar, A., J. Suresh Babu, A. Harikrishna, L. Rajeshkumar, and V. Sathiyamoorthy. Optimization of cutting zone temperature in machining of magnesium alloy using Taguchi method. In *Technology Innovation in Mechanical Engineering*, Springer, Singapore, 2022, pp. 459–468.

[62] Dinesh Kumar, S., K. Muthukumar, and S. Karthick. Natural inspiration technique for the parameter optimization of A-GTAW welding of naval steel. *Materials Today: Proceedings*, Vol. 21, 2020, pp. 843–846.

[63] Madan, D. Ocean wave energy scenario in India. *International Journal of Mechanical and Production Engineering Research and Development, Special Issue*, 2018, pp. 582–590.

[64] Liu, W., F. Huang, Y. Liao, J. Zhang, G. Ren, Z. Zhuang, et al. Treatment of CrVI-containing Mg(OH)2 nanowaste. *Angewandte Chemie* (*International ed*), Vol. 47, No. 30, 2008, pp. 5619–5622.

[65] Zhang, Z., F. Yang, H. Zhang, T. Zhang, H. Wang, Y. Xu, et al. Influence of CeO2 addition on forming quality and microstructure of TiCx-reinforced CrTi4-based laser cladding composite coating. *Materials characterization*, Vol. 171, 2021, id. 110732.

[66] Qu, M., T. Liang, J. Hou, Z. Liu, E. Yang, and X. Liu. Laboratory study and field application of amphiphilic molybdenum disulfide nanosheets for enhanced oil recovery. *Journal of Petroleum Science and Engineering*, Vol. 208, 2022, id. 109695.

[67] Prabhakaran, S., V. Krishnaraj, S. Sharma, M. Senthilkumar, R. Jegathishkumar, and R. Zitoune. Experimental study on thermal and morphological analyses of green composite sandwich made of flax and agglomerated cork. *Journal of Thermal Analysis and Calorimetry*, Vol. 139, No. 5, 2020, pp. 3003–3012.

[68] Sharma, S., P. Sudhakara, J. Singh, R. A. Ilyas, M. R.M. Asyraf, and M. R. Razman. Critical review of biodegradable and bioactive polymer composites for bone tissue engineering and drug delivery applications. *Polymers*, Vol. 13, No. 16, 2021, id. 2623.

[69] Sharma, S., P. Sudhakara, A. A. B. Omran, J. Singh, and R. A. Ilyas. Recent trends and developments in conducting polymer nanocomposites for multifunctional applications. *Polymers*, Vol. 13, No. 17, 2021, id. 2898.

[70] Jha, K., Y. K. Tyagi, R. Kumar, S. Sharma, M. R. Huzaifah, C. Li, et al. Assessment of dimensional stability, biodegradability, and fracture energy of bio-composites reinforced with novel pine cone. *Polymers*, Vol. 13, No. 19, 2021, id. 3260.

[71] Wang, Y., T. Sun, L. Tong, Y. Gao, H. Zhang, Y. Zhang, et al. Non-free Fe dominated PMS activation for enhancing electro-

Fenton efficiency in neutral wastewater. *Journal of Electroanalytical Chemistry*, Vol. 928, 2023, id. 117062.
[72] Zhao, Y., Q. Li, Q. Cui, and S. Ni. Nitrogen recovery through fermentative dissimilatory nitrate reduction to ammonium (DNRA): Carbon source comparison and metabolic pathway. *Chemical Engineering Journal*, Vol. 441, 2022, id. 135938.
[73] Fan, X., G. Wei, X. Lin, X. Wang, Z. Si, X. Zhang, et al. Reversible switching of interlayer exchange coupling through atomically thin VO2 *via* electronic state modulation. *Matter*, Vol. 2, No. 6, 2020, pp. 1582–1593.
[74] Zhang, Z., Q. Yang, Z. Yu, H. Wang, and T. Zhang. Influence of Y2O3 addition on the microstructure of TiC reinforced Ti-based composite coating prepared by laser cladding. *Materials characterization*, Vol. 189, 2022, id. 111962.
[75] Yang, Y., H. Zhu, X. Xu, L. Bao, Y. Wang, H. Lin, et al. Construction of a novel lanthanum carbonate-grafted ZSM-5 zeolite for effective highly selective phosphate removal from wastewater. *Microporous and Mesoporous Materials*, Vol. 324, 2021, id. 111289.
[76] Singh, G., H. Kumar, and H. K. Kansal. Multi-objective optimization of Chemically assisted Magnetic Abrasive Finishing (MAF) on Inconel 625 tubes using genetic algorithm: Modeling and microstructural analysis. *Micromachines*, Vol. 13, 2022, id. 1168.
[77] Kadier, A., R. A. Ilyas, M. R. Huzaifah, N. Harihastuti, S. M. Sapuan, M. M. Harussani, et al. Use of industrial wastes as sustainable nutrient sources for bacterial cellulose (B. C.) production: mechanism, advances, and future perspectives. *Polymers*, Vol. 13, No. 19, 2021, id. 3365.
[78] Singh, Y., J. Singh, S. Sharma, T.-D. Lam, and D.-N. Nguyen. Fabrication and characterization of coir/carbon-fiber reinforced epoxy based hybrid composite for helmet shells and sports-good applications: influence of fiber surface modifications on the mechanical, thermal and morphological properties. *Journal of Materials Research and Technology*, Vol. 9, No. 6, 2020, pp. 15593–15603.
[79] Suriani, M. J., R. A. Ilyas, M. Y. Zuhri, A. Khalina, M. T. Sultan, S. M. Sapuan, et al. Critical review of natural fiber reinforced hybrid composites: processing, properties, applications and cost. *Polymers*, Vol. 13, No. 20, 2021, id. 3514.
[80] Kumar, R., N. Ranjan, V. Kumar, R. Kumar, J. S. Chohan, A. Yadav, et al. Characterization of friction stir-welded polylactic acid/aluminum composite primed through fused filament fabrication. *Journal of Materials Engineering and Performance*, Vol. 31, 2021, pp. 2391–2409.
[81] Ilyas, R. A., M. Y. M. Zuhri, M. N. F. Norrrahim, M. S. M. Misenan, M. A. Jenol, S. A. Samsudin, et al. Natural fiber-reinforced polycaprolactone green and hybrid biocomposites for various advanced applications. *Polymers*, Vol. 14, No. 1, 2022, id. 182.
[82] Azlin, M. N. M., R. A. Ilyas, M. Y. M. Zuhri, S. M. Sapuan, M. M. Harussani, S. Sharma, et al. 3D printing and shaping polymers, composites, and nanocomposites: a review. *Polymers*, Vol. 14, No. 1, 2022, id. 180.
[83] Chembath, M., J. N. Balaraju, and M. Sujata. Surface characteristics, corrosion and bioactivity of chemically treated biomedical grade NiTi alloy. *Materials Science and Engineering: C*, Vol. 56, 2015, pp. 417–425.
[84] Singh, G., V. Aggarwal, S. Singh, B. Singh, S. Sharma, J. Singh, et al. Experimental investigation and performance optimization during machining of Hastelloy C-276 using green lubricants. *Materials*, Vol. 15, 2022, id. 5451.
[85] Cui, X., C. Li, Y. Zhang, W. Ding, Q. An, B. Liu, et al. A comparative assessment of force, temperature and wheel wear in sustainable grinding aerospace alloy using bio-lubricant. *Frontiers of Mechanical Engineering*, Vol. 18, No. 2, 2022, id. 3.
[86] Xu, W., C. H. Li, Y. Zhang, H. M. Ali, S. Sharma, R. Li, et al. Electrostatic atomization minimum quantity lubrication machining: from mechanism to application. *International Journal of Extreme Manufacturing*, Vol. 4, 2022, pp. 1–43.
[87] Mingzheng, L. I.U., L. I. Changhe, Z. H.A. N.G. Yanbin, Y. A.N. G. Min, G. A.O. Teng, C. U.I. Xin, et al. Analysis of grinding mechanics and improved grinding force model based on randomized grain geometric characteristics. *Chinese Journal of Aeronautics*, 2022, pp. 1–34.
[88] Gao, T., Y. Zhang, C. Li, Y. Wang, Y. Chen, Q. An, et al. Fiber-reinforced composites in milling and grinding: machining bottlenecks and advanced strategies. *Frontiers of Mechanical Engineering*, Vol. 17, No. 2, 2022, id. 24.
[89] Jia, D., Y. Zhang, C. Li, M. Yang, T. Gao, Z. Said, et al. Lubrication-enhanced mechanisms of titanium alloy grinding using lecithin biolubricant. *Tribology International*, Vol. 169, 2022, id. 107461.
[90] Zhang, Y., L. I. Wenyi, T. A. Lizhi, L. I. Changhe, X. Liang, X. U. Shuaiqiang, et al. Abrasive water jet tool passivation: from mechanism to application. *Journal of Advanced Manufacturing Science and Technology*, Vol. 3, No. 1, 2022, id. 2022018.
[91] Wang, X., C. Li, Y. Zhang, H. M. Ali, S. Sharma, R. Li, et al. Tribology of enhanced turning using biolubricants: A comparative assessment. *Tribology International*, Vol. 174, October 2022, id. 107766.
[92] Cui, X., C. Li, Y. Zhang, Z. Said, S. Debnath, S. Sharma, et al. Grindability of titanium alloy using cryogenic nanolubricant minimum quantity lubrication. *Journal of Manufacturing Processes*, Vol. 80, 2022, pp. 273–286.
[93] Duan, Z., C. Li, Y. Zhang, M. Yang, T. Gao, X. Liu, et al. Mechanical behavior and Semiempirical force model of aerospace aluminum alloy Milling using Nano biological lubricant. *Frontiers of Mechanical Engineering*, Vol. 18, No. 3, 2022, id. 4.
[94] Zhang, Z., M. Sui, C. Li, Z. Zhou, B. Liu, Y. Chen, et al. Residual stress of grinding cemented carbide using MoS_2 nano-lubricant. *The International Journal of Advanced Manufacturing Technology*, Vol. 119, No. 9–10, 2022, pp. 5671–5685.
[95] Li, H., Y. Zhang, C. Li, Z. Zhou, X. Nie, Y. Chen, et al. Extreme pressure and antiwear additives for lubricant: academic insights and perspectives. *The International Journal of Advanced Manufacturing Technology*, Vol. 120, No. 1–2, 2022, pp. 1–27.
[96] Wu, X., C. Li, Z. Zhou, X. Nie, Y. Chen, Y. Zhang, et al. Circulating purification of cutting fluid: an overview. *The International Journal of Advanced Manufacturing Technology*, Vol. 117, No. 9–10, 2021, pp. 2565–2600.
[97] Gao, T., Y. Zhang, C. Li, Y. Wang, Q. An, B. Liu, et al. Grindability of carbon fiber reinforced polymer using CNT biological lubricant. *Scientific Reports* (*Nature*), Vol. 11, 2021, id. 22535.

[98] Tang, L., Y. Zhang, C. Li, Z. Zhou, X. Nie, Y. Chen, et al. Biological stability of water-based cutting fluids: progress and application. *Chinese Journal of Mechanical Engineering*, Vol. 35, 2022, id. 3.

[99] Gao, T., C. Li, Y. Wang, X. Liu, Q. An, H. N. Li, et al. Carbon fiber reinforced polymer in drilling: From damage mechanisms to suppression. *Composite Structures*, Vol. 286, 2022, id. 115232.

[100] Liu, M., C. Li, Y. Zhang, Q. An, M. Yang, T. Gao, et al. Cryogenic minimum quantity lubrication machining: from mechanism to application. *Frontiers of Mechanical Engineering*, Vol. 16, 2021, pp. 649–697.

[101] Wang, X., C. Li, Y. Zhang, Z. Said, S. Debnath, S. Sharma, et al. Influence of texture shape and arrangement on nanofluid minimum quantity lubrication turning. *The International Journal of Advanced Manufacturing Technology*, Vol. 119, 2022, pp. 631–646.

[102] Li, H., Y. Zhang, C. Li, Z. Zhou, X. Nie, Y. Chen, et al. Cutting fluid corrosion inhibitors from inorganic to organic: Progress and applications. *Korean Journal of Chemical Engineering*, Vol. 39, No. 5, 2022, pp. 1107–1134.

[103] Xin, C. U., L. I. Changhe, D. I. Wenfeng, C. H. Yun, M. A. Cong, X. U. Xuefeng, et al. Minimum quantity lubrication machining of aeronautical materials using carbon group nanolubricant: From mechanisms to application. *Chinese Journal of Aeronautics*, Vol. 35, No. 11, 2021, pp. 85–112.

[104] Singh, J., S. S. Gill, M. Dogra, R. Singh, M. Singh, S. Sharma, et al. State of the art review on the sustainable dry machining of advanced materials for multifaceted Engineering applications: Progressive advancements and directions for future prospects. *Materials Research Express*, Vol. 9, 2022, pp. 1–25.

[105] Singh, J., S. S. Gill, M. Dogra, S. Sharma, M. Singh, S. P. Dwivedi, et al. Effect of Ranque-Hilsch vortex tube cooling to enhance the surface-topography and tool-wear in sustainable turning of Al-5.6Zn-2.5Mg-1.6Cu-0.23Cr-T6 aerospace alloy. *Materials*, Vol. 15, No. 16, 2022, id. 5681.

[106] Khan, A. M., M. Alkahtani, S. Sharma, M. Jamil, A. Iqbal, and N. He. Sustainability-based holistic assessment and determination of optimal resource consumption for energy-efficient machining of hardened steel. *Journal of Cleaner Production*, Vol. 319, 2021, id. 128674.

[107] Roslan, Z. B., Z. Ramli, M. R. Razman, M. R. M. Asyraf, M. R. Ishak, R. A. Ilyas, et al. Reflections on local community identity by evaluating heritage sustainability protection in Jugra, Selangor, Malaysia. *Sustainability*, Vol. 13, 2021, id. 8705.

[108] Asyraf, M. R., M. R. Ishak, M. N. Norrrahim, N. M. Nurazzi, S. S. Shazleen, R. A. Ilyas, et al. Recent advances of thermal properties of sugar palm lignocellulosic fibre reinforced polymer composites. *International Journal of Biological Macromolecules*, Vol. 193, 2021, pp. 1587–1599.

[109] Asyraf, M. R. M., M. Rafidah, A. Azrina, and M. Razman. Dynamic mechanical behaviour of kenaf cellulosic fibre biocomposites: a comprehensive review on chemical treatments. *Cellulose*, Vol. 28, 2021, pp. 1–21.

[110] Ali, S. S. S., M. R. Razman, A. Awang, M. R. M. Asyraf, M. R. Ishak, R. A. Ilyas, et al. Critical determinants of household electricity consumption in a rapidly growing city. *Sustainability*, Vol. 13, 2021, id. 4441.

[111] Asyraf, M. R., M. R. Ishak, A. Syamsir, N. M. Nurazzi, F. A. Sabaruddin, S. S. Shazleen, et al. Mechanical properties of oil palm fibre-reinforced polymer composites: a review. *Journal of Materials Research and Technology*, Vol. 17, 2022, pp. 33–65.

[112] Khan, A. M., S. Anwar, A. Alfaify, M. Jamil, S. Sharma, M. U. Farooq, et al. Comparison of machinability and economic aspects in turning of Haynes-25 alloy under novel hybrid cryogenic-LN oils-on-water approach. *The International Journal of Advanced Manufacturing Technology*, Vol. 120, 2022, pp. 427–445.

[113] Rahman, M. A., M. S. Bhuiyan, S. Sharma, M. S. Kamal, M. M. Imtiaz, A. Alfaify, et al. Influence of feed rate response (FRR) on chip formation in micro and macro machining of al alloy. *Metals*, Vol. 11, No. 1, 2021, id. 159.

[114] Ganeshkumar, S., B. K. Singh, S. D. Kumar, S. Gokulkumar, S. Sharma, K. Mausam, et al. Study of wear, stress and vibration characteristics of silicon carbide tool inserts and nano multi-layered titanium nitride-coated cutting tool inserts in turning of SS304 steels. *Materials*, Vol. 15, No. 22, 2022, id. 7994.

[115] Singh, M., S. Sharma, A. Muniappan, D. Y. Pimenov, S. Wojciechowski, K. Jha, et al. In situ micro-observation of surface roughness and fracture mechanism in metal microforming of thin copper sheets with newly developed compact testing apparatus. *Materials*, Vol. 15, No. 4, 2022, id. 1368.

[116] Bai, X., J. Jiang, C. Li, L. Dong, H. M. Ali, S. Sharma. Tribological performance of different concentrations of Al2O3 nanofluids on minimum quantity lubrication milling. *Chinese Journal of Mechanical Engineering*, Vol. 36, 2023, id. 1368.